

A ONE-DIMENSIONAL FLUX-BASED THERMOGRAPHY FOR THERMAL
DIFFUSIVITY ESTIMATION IN METALLIC ALLOYS

by

Ahmed Elsheikh

A Thesis Presented to the Faculty of the
American University of Sharjah
College of Engineering
in Partial Fulfillment
of the Requirements
for the Degree of

Master of Science in
Mechanical Engineering

Sharjah, United Arab Emirates

October 2022

Declaration of Authorship

I declare that this thesis is my own work and, to the best of my knowledge and belief, it does not contain material published or written by a third party, except where permission has been obtained and/or appropriately cited through full and accurate referencing.

Signature **Ahmed Elsheikh**

Date **10/17/22**

The Author controls copyright for this report.
Material should not be reused without the consent of the author. Due
acknowledgement should be made where appropriate.

© Year 2022

Ahmed Elsheikh

ALL RIGHTS RESERVE

Approval Signatures

We, the undersigned, approve the Master's Thesis of Ahmed Elsheikh

Thesis Title: A one-dimensional flux-based thermography for thermal diffusivity estimation in metallic alloys

Date of Defense: 10/17/2022

Name, Title and Affiliation

Signature

Dr. Bassam A. Abu-Nabah
Associate Professor, Department of Mechanical
Engineering
Thesis Advisor

Dr. Mohammad O. Hamdan
Professor, Department of Mechanical Engineering
Thesis Co-Advisor

Dr. Mohamed Abdelgawad
Associate Professor, Department of Mechanical
Engineering
Thesis Committee Member

Dr. Rami Haweeleh
Professor, Department of Civil Engineering
Thesis Committee Member

Dr. Mamoun F. Abdel-Hafez
Head
Department of Mechanical Engineering

Dr. Lotfi Romdhane
Associate Dean for Graduate Affairs and Research
College of Engineering

Dr. Fadi Aloul
Dean
College of Engineering

Dr. Mohamed El-Tarhuni
Vice Provost for Graduate Studies
Office of Research and Graduate Studies

Acknowledgments

To start with, I would like to express my sincere gratitude to my advisors Dr. Bassam A. Abu-Nabah and Dr. Mohamed O. Hamdan for guiding me throughout the different stages of this research. I would like to specially thank Dr. Bassam A. Abu-Nabah for his immense support, knowledge, mentorship, persuasion, and patience, and also for introducing me to the enjoyable nondestructive testing and evaluation field.

Furthermore, I would like to thank the thesis examination committee members, Dr. Mohamed Abdelgawad and Dr. Rami Haweeleh for the thoughtful discussions, insightful comments, and invaluable feedback.

I would also like to express my appreciation to the Mechanical Engineering department for allowing this work possible through funding this research, granting me the graduate research assistantship, and allowing me to use the American University of Sharjah's resources. The graduate research assistantship granted me invaluable technical and soft skills.

Last but not least, I would like to express my utmost admiration for my family and friends for supporting me, believing in me, and being a ceaseless source of inspiration.

Dedication

To my family...

Abstract

This work proposes a simple one-dimensional (1D) thermography technique to estimate a metallic alloy thermal diffusivity by employing a uniform flux-based heating source. A theoretical model is developed and validated to account for the sample dimensions, material thermal properties and the sample initial and boundary conditions. These conditions include the sample initial temperature, the effective convection heat transfer coefficient with the surrounding environment and the uniform heat flux supplied to the sample. The adopted theoretical model is tested against simulated thermal measurements to retrieve a sample unknown boundary conditions along with the material thermal diffusivity of interest following the Nelder-Mead optimization approach, which offers a high flexibility to the proposed technique. This technique is experimentally validated over a tempered aluminum alloy (Al-2024 T4) of relatively high thermal diffusivity and a one-order of magnitude lower thermal diffusivity annealed stainless-steel alloy (SS-304) delivering an uncertainty lower than 2% in material thermal diffusivity estimation.

Keywords: Thermal diffusivity; heat diffusion; thermography; infrared; nondestructive testing and evaluation

Table of Contents

Abstract	6
Table of Contents	7
List of Figures	8
List of Tables	10
List of Abbreviations	11
Chapter 1. Introduction	13
1.1. Introduction	13
1.2. Overview	13
1.3. Thesis Objectives	14
1.4. Research Contribution	14
1.5. Thesis Organization	15
Chapter 2. Background and Literature Review	16
2.1. Non-thermography Methods	16
2.2. Thermography Methods	18
Chapter 3. Methodology	24
3.1. Forward Theoretical Model	24
3.2. Thermal Diffusivity Estimation	27
Chapter 4. Model Validation	29
4.1. Forward Model Validation	29
4.2. FEA Mesh Independence	32
4.3. Validation of Thermal Diffusivity Estimation	35
Chapter 5. Experimental Setup	39
5.1. Sample Design	39
5.2. Emissivity Check	39
5.3. Thermography System	42
5.4. Experimental Procedure	44
Chapter 6. Results and Discussion	47
Chapter 7. Summary and Future Work	52
7.1. Conclusion	52
7.2. Future Work	52
References	54
Vita	62

List of Figures

- Figure 2-1: A schematic representation of (a) the absolute technique and (b) the radial flow method [14]. 17
- Figure 2-2: A schematic representation of (a) the steady-state method and (b) the 3ω method [14]. 17
- Figure 2-3: (a) Flash thermography [25] and (b) Laser flash thermography [31] setups. 19
- Figure 2-4: (a) Laser spot thermography [2] and (b) Laser line thermography [44] setups. 20
- Figure 2-5: (a) Flux-based thermography [47] and (b) Hot-rod thermography [48] setups. 23
- Figure 3-1: A schematic representation of the heat transfer model showing the effective convection heat transfer losses to the surrounding environment from exposed fin surfaces while applying a uniform heat flux at the base (left side). 25
- Figure 3-2: A schematic flowchart representation of the Nelder-Mead optimization approach in estimating three-unknown vector $V = (\alpha, Bi, \bar{q}'')^T$ in this study. 28
- Figure 4-1: Estimated temperature change at different timeframes using the theoretical model (solid lines) and FE simulations (empty markers) over (a) Al-2024 and (b) SS-304 samples. 30
- Figure 4-2: RMSE trend of theoretically estimated temperature change using different N number of terms ranging between 1 and 100 over (a) Al-2024 and (b) SS-304 samples. 31
- Figure 4-3: Schematic representation of the mesh independence study of the 3D FEA COMSOL simulation of the Al-2024 sample showing (a) extremely coarse, (b) coarse, (c) fine, and (d) extremely fine mesh sizes. 33
- Figure 4-4: Estimated temperature change at different timeframes using the theoretical model (solid lines) and FE simulations (empty markers) over Al-2024 using (a) extremely coarse, (b) coarse, (c) fine, and (d) extremely fine mesh sizes. 34

- Figure 4-5: The convergence of estimated (a) dimensionless heat flux, (b) Biot number, (c) thermal diffusivity and (d) error in thermal diffusivity estimation with iterations using Al-2024 FE simulated data. 36
- Figure 4-6: The convergence of estimated (a) dimensionless heat flux, (b) Biot number, (c) thermal diffusivity and (d) error in thermal diffusivity estimation with iterations using SS-304 FE simulated data. 37
- Figure 4-7: The criteria for selecting the least N number of terms needed to reduce the thermal noise $\Delta\theta_n$ effect in thermal diffusivity estimation over FE simulated thermal data for (a) Al-2024 and (b) SS-304. 38
- Figure 5-1: Emissivity check of the Plasti Dip black rubber coating using a thermal tape on five different locations shown by (a) the visible image and (b) the thermal image 42
- Figure 5-2: A presentation of (a) the experimental setup used in this study and (b) the strip heater in contact with the sample's left side. 43
- Figure 5-3: Thermal images $\theta(x, y, t)$ captured at different timeframes for (a) Al-2024 and (b) SS-304 samples. 46
- Figure 6-1: Average temperature change $\theta(x, t)$ at different timeframes using the theoretical model (solid lines) and experimental data (solid markers) over (a) Al-2024 and (b) SS-304 samples. 48
- Figure 6-2: Experimental uncertainty in thermal diffusivity estimation of the (a) Al-2024 and (b) SS-304 samples using different N number of terms. 50
- Figure 6-3: The convergence in experimental thermal diffusivity estimation of the (a) Al-2024 and (b) SS-304 samples with iterations. 50

List of Tables

Table 2-1: Summary of IR thermal diffusivity estimation techniques, assumptions, materials and absolute uncertainties reported in the literature.	22
Table 4-1: FE simulation parameters and samples dimensions.	29
Table 5-1: Reported emissivity values of the rubber coating over 10 repetitions.	42
Table 5-2: Thermography setup parameters.	44
Table 6-1: Summary of experimental thermal diffusivity estimates and their uncertainties.	51

List of Abbreviations

Abbreviations

Al – Aluminum

ARSS - Average Residual Sum of Squares

ASTM – American Society for Testing and Materials

CTM – Contact Thermometer Method

DC – Direct Current

ECT – Eddy Current Thermography

FBT – Flux-based Thermography

FEA – Finite Element Analysis

FOV – Field of View

FT – Flash Thermography

HRT – Hot-rod Thermography

IR – Infrared

IRT – Infrared Thermography

LFT – Laser Flash Thermography

LPST – Lamp Spot Thermography

LST – Laser Spot Thermography

LLT – Laser Line Thermography

LT – Lock-in Thermography

NTM – Noncontact Thermometer Method

NDE – Nondestructive Evaluation

NDT&E – Nondestructive Testing and Evaluation

NDT – Nondestructive Testing

NUC – Non-uniformity Correction

OST – Optically Stimulated Thermography

PT – Pulsed Thermography

RSME – Root Mean Square Error

SH – Step Heating

SS – Stainless Steel

TPS – Transient Plane Source

VT – Vibrothermography

1D – One Dimensional

2D – Two Dimensional

3D – Three Dimensional

Nomenclature

α – Thermal Diffusivity [m^2/s]

k – Thermal Conductivity [$\text{W}/\text{m} \cdot \text{K}$]

c_p – Specific Heat [$\text{J}/\text{kg} \cdot \text{K}$]

h – Effective Convection Heat Transfer Coefficient [$\text{W}/\text{m}^2 \cdot \text{K}$]

Bi – Biot Number

L – Sample Length [mm]

X – Dimensionless Length

ρ – Density [kg/m^3]

T – Temperature [K]

θ – Temperature Difference [K]

q – Induced Heat Flux [kW/m^2]

\bar{q}'' – Dimensionless Heat Flux

Chapter 1. Introduction

1.1. Introduction

This chapter outlines a brief introduction on the importance of evaluating thermal diffusivity of metallic materials in the aerospace sector. The importance of infrared thermography in estimating thermal diffusivity is highlighted with the research contributions being outlined for the proposed technique. Lastly, the organization of the rest of the thesis is described.

1.2. Overview

Thermal diffusivity (α) is a thermal property representing how fast heat diffuses through a material due to an induced temperature difference [1]. In essence, thermal diffusivity is expressed as the ratio of thermal conductivity to the volumetric heat capacity of a material. Accordingly, metallic alloys with high thermal diffusivity will have high heat conduction rates with respect to their heat storage capacities allowing heat to propagate faster in such media. Industries with applications involving the operation of mechanical and electrical components under heat transfer conditions mandate accurate estimation of the material thermal diffusivity being used [2]–[4]. At present, various techniques exist for assessing the thermal diffusivities of different material types and physical forms such as gases, liquids, powders, coatings, composites and metals [5].

Generally, aluminum alloys are extensively adopted in the aerospace and aviation fields due to their high strength-to-weight ratio when compared to other metals [6], [7]. Particularly, Al-2024 has secured its position as the lead material in the manufacturing of aircraft airfoils, wings, and fuselages since its material composition enables it to sustain the highest hardness amongst the other aluminum alloys [8]. Moreover, the estimation of thermal diffusivity falls under the design and manufacturing of aerospace structural components at different heat transfer conditions. When deployed, aircraft structures sustain cyclic loading or fatigue which can result in crack initiation and propagation over time. Hence, it is crucial to detect cracks and estimate their sizes to assess the magnitude of the damage and whether the structure needs replacement or not. Eddy current thermography [9] and vibrothermography [10], [11] are rapidly evolving nondestructive evaluation techniques for detecting and estimating surface and sub-surface manifested cracks in metallic alloy aircraft components. The induced vibration causes heat generation along the crack, mainly due to frictional heating [12], [13], while

an infrared camera captures the generated heat profile. Crack size evaluation using thermography inspection techniques relies on multiple parameters including the material thermal diffusivity under inspection. Therefore, developing a simple technique to estimate the thermal diffusivity is vital to the aerospace industry.

1.3. Thesis Objectives

Several efforts have been made to identify the thermal diffusivities of metallic samples. Infrared Thermography (IRT) which is a rapid and accurate nondestructive testing and evaluation (NDT&E) technique, is a commonly employed practice in the aerospace industry. To independently estimate a material thermal diffusivity with accuracy is rather expensive, time consuming and mandates the implementation of numerous experimental constraints. In contrast, this work proposes a simple one-dimensional (1D) active thermography technique to estimate a metallic alloy thermal diffusivity by employing a uniform flux-based heating source.

1.4. Research Contribution

The summary of the contributions of this research work is listed below as follows:

- Develop a forward theoretical model to account for the sample dimensions, material thermal properties, effective heat convection coefficient with the surrounding environment and a uniform heat flux applied to the sample.
- Validate the accuracy of the forward theoretical model using finite element simulations performed on commercially available software.
- Utilize the Nelder-Mead optimization approach with the adopted theoretical model to estimate the material thermal diffusivity of interest along with the applied heat flux and effective convection heat transfer coefficient with the surrounding environment.
- Implement experimental emissivity check on the tested samples following the Noncontact Thermometer Method (NTM) defined by the American Society for Testing and Materials (ASTM).
- Perform the proposed experimental IRT technique on a tempered aluminum alloy (Al-2024 T4) of relatively high thermal diffusivity and a one-order of magnitude lower thermal diffusivity annealed stainless-steel alloy (SS-304).

1.5. Thesis Organization

This thesis report is organized into the following chapters: Chapter 2 discusses a thorough literature review about the different non-thermography and thermography nondestructive testing (NDT) methods to evaluate the thermal diffusivity of a given metallic material. Chapter 3 demonstrates the forward theoretical mathematical model behind the suggested technique along with the numerical estimation technique implemented to evaluate the material thermal diffusivity. In Chapter 4, the forward 1D theoretical model is validated in a close comparison with its corresponding 3D finite element simulation, which is then used to retrieve a material thermal diffusivity from the simulated temperature change along the samples. The sample design, the thermography setup, the emissivity check, and the experimental procedure used in this study are presented in Chapter 5. Chapter 6 presents the results and level of accuracy obtained of the estimated thermal diffusivity from the proposed method. Finally, Chapter 7 outlines the summary, conclusion, and future work on this thesis.

Chapter 2. Background and Literature Review

This chapter discusses the different non-thermography and thermography techniques in estimating material thermal diffusivity, available in literature. Non-thermography methods usually employ thermocouples that come in contact with the samples under study, while thermography techniques employ thermal infrared cameras to capture the temperature of the samples under examination.

2.1. Non-thermography Methods

Material thermal characterization measurement methods, either on bulk samples or thin films, are categorized into two classes: steady state techniques and transient techniques. Self-explanatory, the steady state methods impose a consistent temperature difference across the sample that does not vary with time. Contrarily, transient methods impose a time-dependent energy profile. In their review, Zhao *et al.* [14] discuss different steady and transient contact methods to measure thermal conductivity, which could be extended to measure thermal diffusivity instead. The absolute technique, a steady state method, is a measuring technique applied on bulk rectangular or cylindrical samples placed between a heat source and a sink while thermocouples act as sensors measuring the temperature difference, as shown in Figure 2-1(a). To obtain accurate temperature readings from the thermocouples, precautions have to be taken into consideration. Measurements are preferred to be conducted under vacuum conditions to minimize convective heat losses [15]; as well as, thin thermocouple wires have to be used to minimize the conductive heat losses [16]. The absolute technique is reasonable at low temperatures, but when it comes to measurements at very high temperatures, the radial heat flow method is more suitable. This method, requires a lower surface area geometry as heat losses to the environment cannot be ignored, that is why cylindrical geometry samples are used [17], as shown in Figure 2-1(b). To overcome many drawbacks of the steady state measurement methods for bulk materials, a transient method called the pulsed power technique was first developed by Maldonado [18]. Similar to the absolute technique, this method incorporates periodical heating for the heating current, while maintaining same apparatus and geometrical sample as the latter one. Also, the transient plane source (TPS) method, is a transient measurement technique which uses a thin metal strip as the heat source and sensor, sandwiched between the thin testing slabs [19].

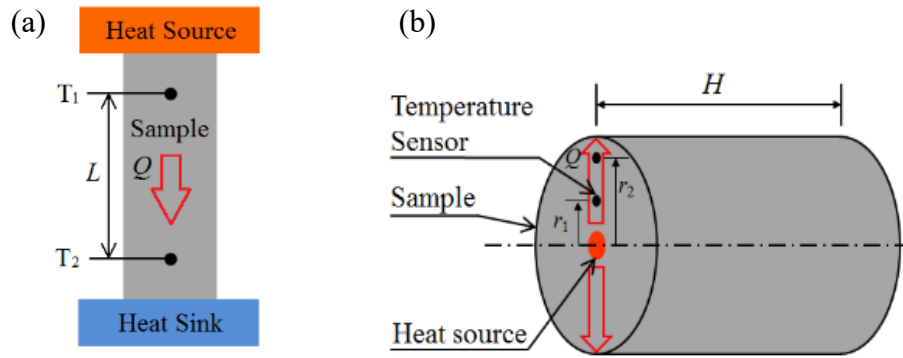


Figure 2-1: A schematic representation of (a) the absolute technique and (b) the radial flow method [14].

While the above methods have been developed to mostly measure thermal conductivities or diffusivities of bulk metallic samples, several methods have been developed to measure the in-plane and cross-plane thermal diffusivities of thin metallic films. Categorized into steady-state and transient techniques, the most frequent steady-state technique which measures the cross-plane thermal diffusivity involves the placing of metallic strips on the film deposited on a highly conductive substrate [14]. This metallic strip is then heated by a direct current (dc) passing through it while also measuring its own temperature, acting as both an electrical heater and sensor, shown in Figure 2-2(a). Furthermore, a similar technique has been utilized to measure the steady-state in-plane thermal diffusivity by Volklein *et al.* [20]; however, evaluating heat flow along the film is a major drawback in this technique, thus parasitic heat losses have to be minimized for an accurate measurement. Conversely, one of the most common transient methods of measuring thermal properties is the 3ω method, displayed in Figure 2-2(b). This technique is widely implemented to measure both bulk and thin films' thermal diffusivities where the intended film is placed on a substrate while a metallic strip heats and senses the heat flow [21], [22].

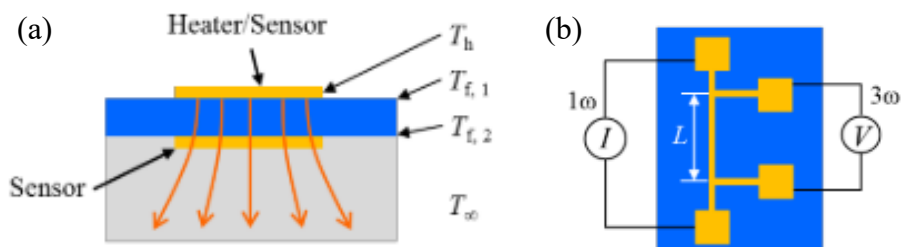


Figure 2-2: A schematic representation of (a) the steady-state method and (b) the 3ω method [14].

2.2. Thermography Methods

Infrared (IR) thermography, an accurate and robust nondestructive evaluation (NDE) technique with many variations, is a common method to estimate a material thermal diffusivity in the aerospace industry. It involves the use of a thermal IR camera to monitor and capture the thermal profile generated on the sample from a heating source. IR thermography methods are grouped into two classes, namely passive and active thermography. Passive thermography benefits from the heat already present in the environment, while active thermography employs an external heating source to thermally excite the sample creating the required thermogram. Active thermography methods are further classified into four categories, namely lock-in thermography (LT), pulsed thermography (PT), step heating (SH), and vibrothermography (VT). LT techniques imply the periodic heating of the sample's surface through a modulated heating source at a certain frequency till a steady state heating pattern is reached [23]. PT methods implicate short heat pulses produced by a high power energy source exciting the sample's surface. Subsequently, the generated thermal profile is captured using the IR camera and examined in the transient regime [23]. Contrarily, from its name, SH techniques imply a long constant heating pulse or a step heating pattern until a significant temperature difference is experienced by the specimen [24]. Finally, VT involves the application of mechanical vibrations on a specimen, the externally induced vibrations causes heat to be released along defects such as cracks due to frictional heating [24]. Furthermore, active thermography methods could be further categorized depending on the type of heating source used, namely optical or non-optical heating sources.

Considered as the most common active thermography technique, flash thermography (FT) is an optical PT technique first developed utilizing a xenon flash lamp to excite the surfaces of multiple metallic samples [25]. In flash thermography, also known as two-sided flash thermography, the sample's surface is excited from one side while the IR camera monitors the transient thermal response on the other side, allowing for the estimation of the sample's through-thickness thermal properties such as thermal diffusivity, conductivity, and heat capacity, as presented by Figure 2-3(a). Furthermore, the classical two-sided FT technique was used to measure the in-plane thermal

diffusivity of the metallic sample under study [26]. Moreover, the typical flash technique was modified to a single-sided method where the excitation and recording of the sample are done on the same side to estimate the thermal diffusivity of multiple metallic and composite slabs [27], [28].

Apart from the classical flash technique, laser flash thermography (LFT) follows the same procedure but replaces the xenon flash lamp by a laser source to excite the entire surface of the specimen, as shown in Figure 2-3(b). A two-sided configuration has been implemented to estimate the thermal diffusivities of stainless-steel [4], austenitic steel [29], and iron and ceramic disks [30]. In addition, a single sided configuration of the LFT method has been developed to estimate the thermal diffusivities of metallic, ceramic, and polymeric thin plates [31], while the two-sided method was employed to characterize thin metallic, polymeric, and composite films [32]. It should be noted that black paint or graphite soot was sprayed on all metallic samples in the majority of the aforementioned studies to enhance the surface emissivity.

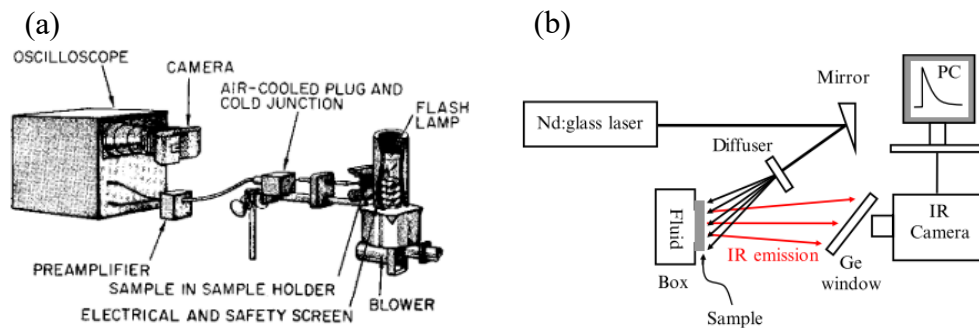


Figure 2-3: (a) Flash thermography [25] and (b) Laser flash thermography [31] setups.

Laser thermography is another widely used technique to estimate thermal diffusivity of diverse materials. It is an active thermography method that illuminates a specific region on the sample's surface, opposed to flash thermography that excites the entire surface, using laser spot thermography (LST) or laser line thermography (LLT) techniques. Categorized into single-sided and two-sided methods, LST involves a laser beam, usually of Gaussian shape, that excites a spot on the sample's surface, presented by Figure 2-4(a). Multiple single-sided LST methods have been proposed in the literature to estimate thermal diffusivities of metallic and composite thin plates [33], thin metallic films [34], stainless-steel disks [35], metallic, polymeric, ceramic slabs [36]–[38], porous stones [39], and semiconductor slabs [40]. Similarly, a two-sided LST

configuration has been implemented to evaluate thermal diffusivities of different metallic and ceramic thin plates [2], [41], [42]. Also, this configuration was used to characterize metallic, composite and polymeric foils, films and wires [43]. Unlike LST, LLT involves a laser line beam instead of spot to excite part of the specimen's surface as shown in Figure 2-4(b), where it has been used to estimate material thermal diffusivity of thin metallic and polyimide films [44], and different metallic, composite and polymeric filaments [45]. Similar to the flash technique, most reported studies using laser thermography have coated all shiny surfaces of metals and ceramics using black paint, colloidal graphite, or dry graphite to improve the absorptivity and emissivity of these surfaces.

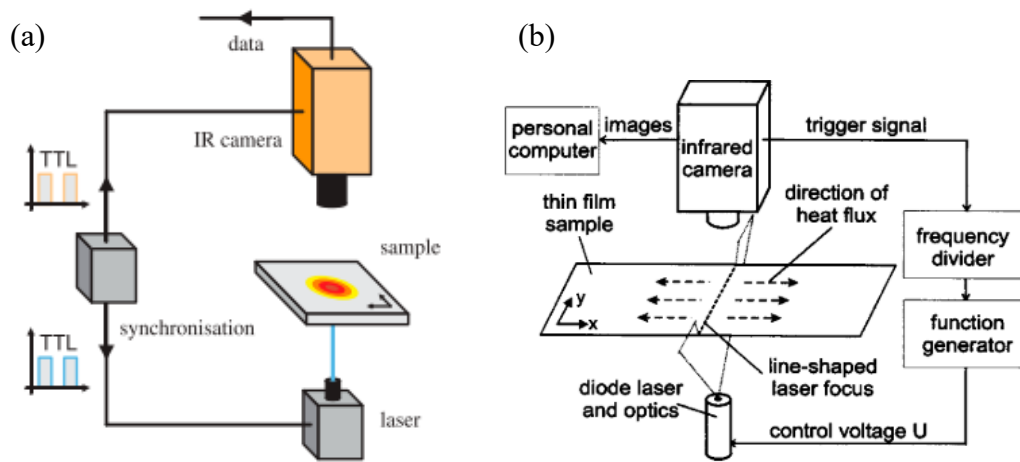


Figure 2-4: (a) Laser spot thermography [2] and (b) Laser line thermography [44] setups.

Apart from the flash and laser thermography techniques, few methods have been developed using a novel energy source to excite or heat the specimens. For instance, an optical method named the lamp spot thermography (LPST) was developed, where a lamp was used to flash a slab of stainless-steel to measure the in-plane thermal diffusivity of the specimen [46]. In addition, flux-based thermography (FBT), a non-optical SH technique shown in Figure 2-5(a), involves a thermal gun continuously heating the front surfaces of aluminum, copper and brass slabs that were roughened using emery paper to ensure uniform surface finish, while an IR camera captures the heat print of the back surface to estimate the thermal diffusivity of the materials [47]. Another approach that utilized a novel heat source to excite the specimen follows a two-sided thermography configuration in which the back side of the specimen is heated

using a hot rod that comes in contact with a stainless-steel slab, while an IR camera monitors the temperature distribution of the black-coated front side to estimate the thermal diffusivity [48], was named as Hot-rod thermography (HRT) and displayed in Figure 2-5(b). Table 2-1 summarizes all thermography methods discussed above along with their assumptions, estimation techniques, materials tested, and errors in thermal diffusivity estimates.

Most of the developed techniques discussed earlier and summarized in Table 2-1 require complicated experimental setups to evaluate the thermal diffusivity of a specimen under study and/or an accurate control of the power being supplied to the excitation source. In contrast, this work proposes a simple one-dimensional (1D) SH active thermography technique to estimate a metallic alloy thermal diffusivity by employing a uniform flux-based heating source. A forward theoretical model is developed to account for the sample dimensions, material thermal properties, effective heat convection coefficient with the surrounding environment and a uniform heat flux applied to the sample. The accuracy of the forward theoretical model is validated using finite element simulations, and the results confirm its efficacy in estimating the material thermal diffusivity from simulated measurement. The proposed method is advantageous as it requires no information on the applied heat flux nor the effective convection heat transfer coefficient with the surrounding environment as the adopted theoretical model is used to estimate these parameters along with the material thermal diffusivity of interest following the Nelder-Mead optimization approach. Numerical optimization algorithms are adopted whenever multiple thermal properties are simultaneously estimated, most common is the estimation of thermal diffusivity and heat loss coefficient, which is evident through the estimation techniques summarized in Table 2-1. This proposed technique is tested experimentally over an aluminum alloy (Al-2024 T4) of relatively high thermal diffusivity and a one-order of magnitude lower thermal diffusivity using an annealed stainless-steel alloy (SS-304) delivering an uncertainty lower than 2% in material thermal diffusivity estimation.

Table 2-1: Summary of IR thermal diffusivity estimation techniques, assumptions, materials and absolute uncertainties reported in the literature.

Technique	Assumptions – Estimation	Material	Uncertainty
FT [25]	1D Model: h (ignored) – A	Al, Ni, Ag, Sn, Zn, St, Cu, Fe and Ti alloys	10% *
FT [27]	1D Model: h (ignored) – NO	SS and Teflon	25% – 45% **‡
FT [26]	2D Model: h (estimated) – NO	Al alloy	5.20% *‡
LFT [4]	1D Model: $h = 0$ (vacuum) – N	SS-304	1.22% – 4.15% **‡‡‡‡‡
LFT [29]	1D Model: $h = 0$ (vacuum) – A	Austenitic St	1.70% *‡
LFT [31]	1D Model: h (estimated) – NO	Cu, Ni, Zn, Pb, SS-304, Ceramics and Polymers	3% – 10% **‡
LFT [30]	3D Model: $h = 0$ (vacuum) – N	Armco Iron and Pyrocream	3% – 5% *‡
LST [33]	1D Model: h (estimated) – NO	SS, Brass, Al 2024-T6 and Graphite fiber composite	10% *
LST [37]	1D Model: h (ignored) – N	SS-2343, Sn, Brass and Textolite	3% – 13.84% *‡
LST [2]	1D Model: $h = 0$ (vacuum) – N	St-1403, SS-304 and Brass	1.32% – 3.95% **‡‡
LST [42]	2D Model: h (ignored) – A	St and Alumina	3% *
LST [36]	2D Model: h (ignored) – N	SS-304, Pb, Ceramics, Polymers and Composites	5% **‡‡‡‡‡
LST [45]	2D Model: $h = 0$ (vacuum) – N	SS-302, Cu, Ni, Ceramics, Polymers and Hair	5% **‡‡‡‡‡
LST [41]	3D Model: h (ignored) – A	Al, Ni and Ceramics	10% *‡
LST [39]	3D Model: h (ignored) – N	SS-304 and Stones	0.25% – 7.87% **‡
LST [40]	3D Model: h (ignored) – A	SiC and Glass fiber composite	5.12% *
LST [34]	3D Model: h (ignored) – N	Inox-304L and Ni	5% **‡
LST [35]	3D Model: h (assumed) – N	SS-304	0.25% – 1.93% *‡
LST [38]	3D Model: h (estimated) – NO	SS-304, Graphite, PEEK and Ceramics	5% **‡
LLT [44]	1D Model: h (estimated) – NO	Cu-ETP, Ni-Ag alloy and Polyimide	10% *‡
LLT [45]	3D Model: $h = 0$ (vacuum) – N	SS-302, Cu, Ni, Ti, Ceramics, Polymers and Hair	5% **‡‡‡‡‡
LPST [46]	3D Model: h (ignored) – N	SS-304	5% – 10% **‡‡‡‡‡
FBT [47]	1D Model: h (assumed) – N	Al, Cu and Brass	1.81% – 5.82% **‡‡
HRT [48]	3D Model: h (ignored) – N	SS-316	1.75% *‡

Estimation: A (Analytical), N (Numerical), and NO (Numerical Optimization)

* is for reported uncertainty in thermal diffusivity estimates

** is for calculated uncertainty from reported thermal diffusivity estimates

‡ is for independent measurement comparison

‡‡ is for literature (technical datasheet) comparison

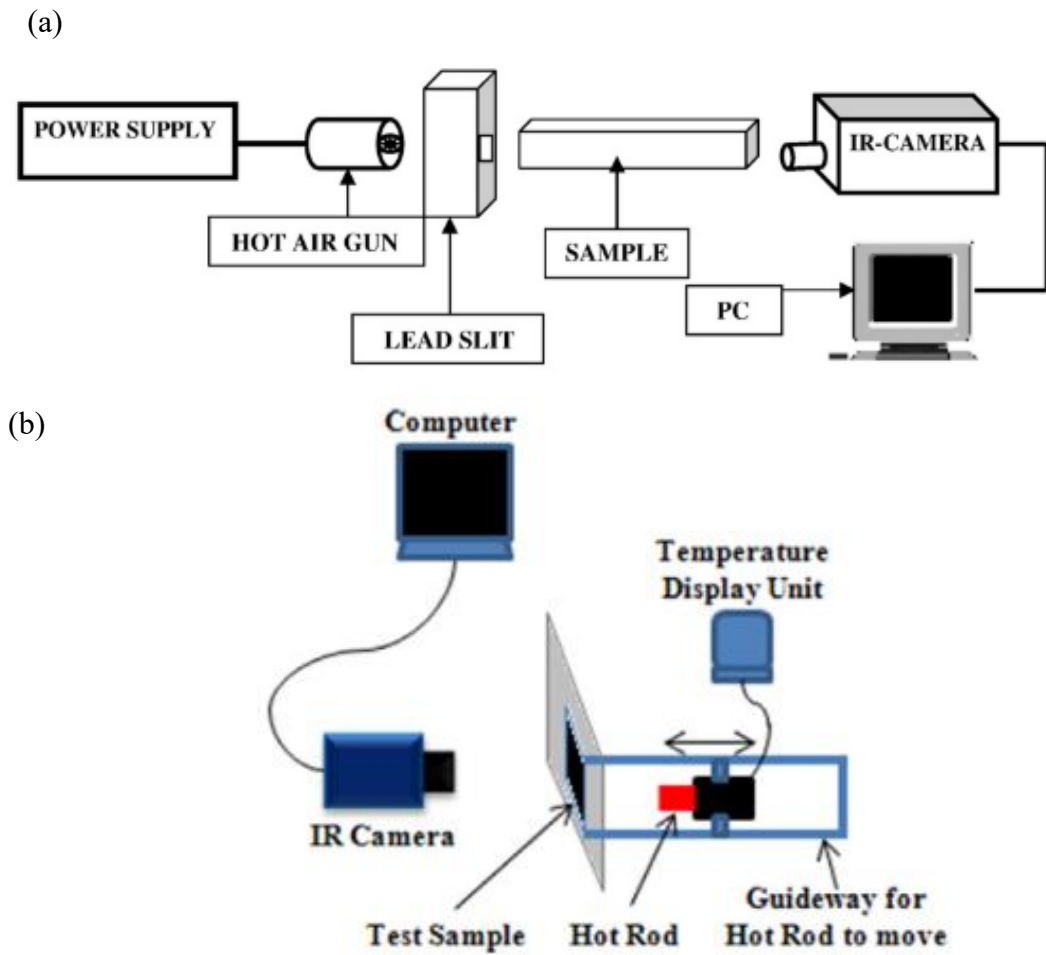


Figure 2-5: (a) Flux-based thermography [47] and (b) Hot-rod thermography [48] setups.

Chapter 3. Methodology

Through the literature review discussed above in Section 2.2 and summarized in Table 2-1, to obtain sub 5% error in thermal diffusivity estimation, complicated models, inaccurate assumptions, and/or sophisticated experimental setups and procedures are equipped. Therefore, a simple and accurate approach to estimate thermal diffusivities of metallic alloys of ranging thermal conductivities is crucial. One of the objectives of this study is to develop a 1D heat diffusion model that accounts for the sample dimensions, material thermal properties, effective heat convection coefficient with the surrounding environment and a uniform heat flux applied to the sample. Through a numerical optimization approach, the thermal diffusivity of the sample, the applied heat flux, and the experienced effective convection coefficient are estimated simultaneously, requiring no prior knowledge on the induced heat flux nor environmental condition, providing high flexibility and robustness to the proposed model.

3.1. Forward Theoretical Model

The proposed forward theoretical model transforms a set of boundary and initial conditions into a prediction of the thermal diffusivity in terms of the temperature change. The heat diffusion through an isotropic material with constant thermal properties follows a model governed by the following partial differential equation (PDE) in rectangular coordinate system:

$$k \left(\frac{\partial^2 T}{\partial x^2} + \frac{\partial^2 T}{\partial y^2} + \frac{\partial^2 T}{\partial z^2} \right) + \dot{e}_{gen} = \rho c_p \frac{\partial T}{\partial t} \quad (1)$$

where ρ , c_p , and k are the material's density, specific heat and thermal conductivity, respectively. \dot{e}_{gen} is the heat generation, while x , y , and z represent the coordinate system for which the temperature T is observed at a certain time t .

For the 1D heat diffusion approximation used in this study, heat is induced from the sample's side diffusing through its length. Accounting for the effective convection heat losses to the surrounding environment along the sample as shown in Figure 3-1, the heat diffusion in the transient regime can be expressed as follows:

$$\frac{\partial^2 T}{\partial x^2} - m^2(T - T_o) = \frac{1}{\alpha} \frac{\partial T}{\partial t} \quad (2)$$

where

$$m^2 = \frac{hP_c}{kA_c} \quad (3)$$

T_0 is the sample initial temperature, which is assumed to be uniform and equal to the surrounding environment temperature T_∞ as the samples are left for a long period of time to stabilize before heat is induced, $\alpha = k/\rho c_p$ is the material thermal diffusivity, and m is a function of the sample's cross-sectional perimeter P_c , cross-sectional area A_c , thermal conductivity k , and the effective convection heat transfer coefficient h with the surrounding environment. The effective convection heat transfer coefficient combines the effect of convection and radiation heat transfer losses endured by the sample to the surrounding environment.

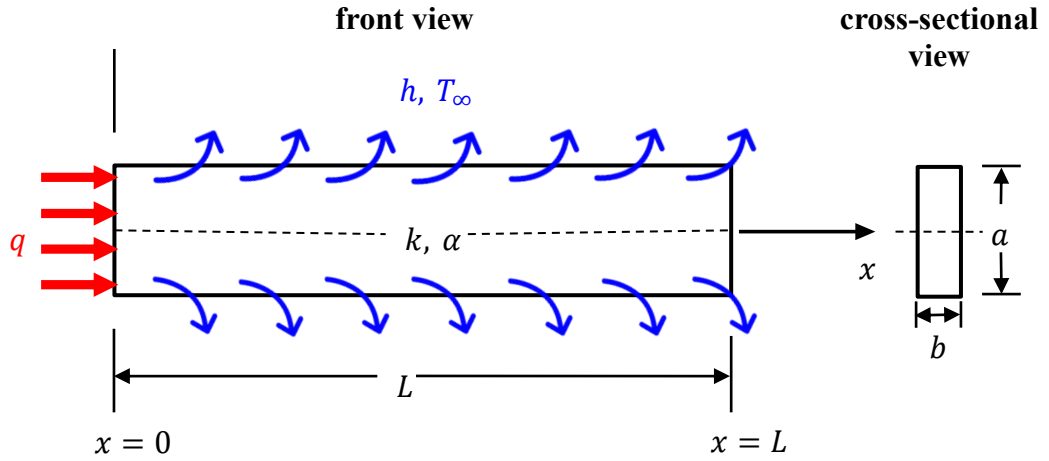


Figure 3-1: A schematic representation of the heat transfer model showing the effective convection heat transfer losses to the surrounding environment from exposed fin surfaces while applying a uniform heat flux at the base (left side).

Considering dimensionless parameters to simplify the solution, the governing model reduces to the following governing model:

$$\frac{\partial^2 \bar{\theta}}{\partial X^2} - \bar{m}^2 \bar{\theta} = \frac{\partial \bar{\theta}}{\partial \tau} \quad (4)$$

where

$$\bar{\theta} = \frac{T - T_0}{T_0} \quad (5)$$

$$X = \frac{x}{L} \quad (6)$$

$$\tau = \frac{\alpha}{L^2} t \quad (7)$$

and

$$\bar{m}^2 = L^2 m^2 \quad (8)$$

where L is the sample length. To solve this PDE problem, a couple of boundary conditions and an initial condition are needed and represented as follows:

$$\frac{\partial \bar{\theta}}{\partial X}(0, \tau) = -\bar{q}'' \quad (9)$$

$$\text{Bi } \bar{\theta}(1, \tau) + \frac{\partial \bar{\theta}}{\partial X}(1, \tau) = 0 \quad (10)$$

and

$$\bar{\theta}(X, 0) = 0 \quad (11)$$

where

$$\text{Bi} = hL/k \quad (12)$$

and

$$\bar{q}'' = (L/kT_o) q \quad (13)$$

Substituting Eqs. (3) and (12) into Eq. (8) delivers $\bar{m}^2 = L^2 m^2 = (P_c L/A_c) \text{Bi}$, where Bi is the Biot number, q is the heat flux, and \bar{q}'' is the dimensionless heat flux.

Solving this PDE in the transient regime results in the following dimensionless solution [49]:

$$\bar{\theta} = \bar{q}'' \left[\frac{1}{\bar{m}} [A \cosh(\bar{m}X) - \sinh(\bar{m}X)] - \sum_{n=1}^{\infty} B_n \cos(\lambda_n X) e^{-(\bar{m}^2 + \lambda_n^2) \tau} \right] \quad (14)$$

where

$$A = \frac{\text{Bi} \sinh(\bar{m}) + \bar{m} \cosh(\bar{m})}{\bar{m} \sinh(\bar{m}) + \text{Bi} \cosh(\bar{m})} \quad (15)$$

$$B_n = \frac{2\lambda_n}{(\bar{m}^2 + \lambda_n^2)(\lambda_n + \cos(\lambda_n) \sin(\lambda_n))} \left[1 + \frac{\lambda_n \sin(\lambda_n) - \text{Bi} \cos(\lambda_n)}{\text{Bi} \cosh(\bar{m}) + \bar{m} \sinh(\bar{m})} \right] \quad (16)$$

and

$$\lambda_n \tan \lambda_n = \text{Bi} \quad (17)$$

To make the solution practical for the proposed measurement approach, Eqs. (5), (7) and (13), are substituted back in Eq. (14) to bring the thermal diffusivity back into the

equation and only estimate the temperature change as observed in the measurement, as follows:

$$\theta = \frac{L}{k} q \left[\frac{1}{\bar{m}} [A \cosh(\bar{m}X) - \sinh(\bar{m}X)] - \sum_{n=1}^N B_n \cos(\lambda_n X) e^{-\frac{\alpha}{L^2}(\bar{m}^2 + \lambda_n^2)t} \right] \quad (18)$$

where

$$\theta = T - T_0 \quad (19)$$

3.2. Thermal Diffusivity Estimation

Direct search methods are numerical techniques that sequentially examine trial solutions through a direct comparison with the current best obtained solution along with a strategy that evaluates a succeeding trial solution [50]. Through the approximation that a given function is continuously differentiable but its derivative is neither reliable nor available, direct search methods are referred to as derivative-free methods as they neither compute nor approximate the gradient of the given function. The most popular of all direct search methods is the Nelder-Mead unconstrained optimization technique [51], which is used in this study and briefly shown in Figure 3-2. Apart from being a simple technique requiring minimal parameters for numerous nonlinear optimization problems, the method implements an optimization algorithm to accelerate the search. The method minimizes an objective function of l variables through the usage of a general geometrical shape “simplex”, such as a tetrahedral having $(l + 1)$ vertices, to replace the vertex with the highest value with another new point. The algorithm allows the simplex to move and reshape adapting to the local landscape by executing a series of geometrical transformations through four basic actions, namely reflection, expansion, contraction, or shrinkage, so that the convergence criteria is met. As it does not require or compute derivatives, the Nelder-Mead direct search method is a convenient choice for optimizing and minimizing objective functions over noisy data, such as the temperature readings taken by an IR camera to computationally estimate the material thermal diffusivity. The 2D transient temperature change readings $\theta(x, y, t)$ taken by the IR camera is averaged along the y dimension resulting in 1D transient temperature change $\theta(x, t)$ along the sample length. The approach is followed to estimate all the three-unknown vector $V = (\alpha, Bi, \bar{q}'')^T$ using the thermal measurements along the sample. This approach iteratively reduces the following

average residual sum of squares (ARSS) objective function until reaching a converged solution:

$$\text{ARSS} = \frac{\sum_{S=1}^S \sum_{p=1}^P \left(\theta_{est}(V, x_p, t_s) - \theta_m(x_p, t_s) \right)^2}{P S} \quad (20)$$

where x_p is the pixel location along the sample at which the temperature change is measured θ_m and estimated θ_{est} at given thermal frame time stamp t_s . P is the number of pixels along the sample and S is the number of time frames in the measurement. Once the ARSS objective function is minimized, the optimized three-unknown vector $V = (\alpha, \text{Bi}, \bar{q}'')^T$ reports the estimated material thermal diffusivity, Biot number, and dimensionless heat flux. In this study, the iterations stop when the relative bounds of the objective function and its corresponding unknowns with iterations reach a tolerance of 1×10^{-4} .

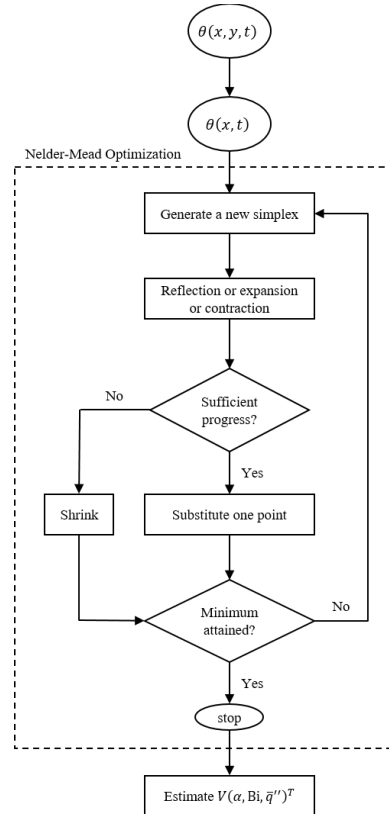


Figure 3-2: A schematic flowchart representation of the Nelder-Mead optimization approach in estimating three-unknown vector $V = (\alpha, \text{Bi}, \bar{q}'')^T$ in this study.

Chapter 4. Model Validation

This section targets the validation of the forward 1D theoretical model, which takes into consideration convective heat transfer losses along the sample, in a close comparison with its corresponding 3D finite element simulation. The validated forward theoretical model is then used to estimate or retrieve a material thermal diffusivity from the simulated temperature change along the sample.

4.1. Forward Model Validation

The heat flux q induced to the samples and the convection heat transfer coefficient h to the surrounding environment were assumed to resemble the experimental testing conditions. The physical and thermal properties of the samples were obtained through the technical datasheets of the experimentally tested samples in this study [52], [53]. Table 4-1 provides all physical and thermal properties of the samples used in this study. Through the use of the forward theoretical model discussed earlier, the transient 1D temperature change along the samples were theoretically estimated from Eqs. (15-18) using MATLAB. The 3D finite element analysis (FEA) was conducted using COMSOL for the same material properties and testing conditions listed in Table 4-1.

Table 4-1: FE simulation parameters and samples dimensions.

		Al-2024 T4 [52]	SS-304 [53]
Properties		Value	
Physical properties	density (ρ)	2780 kg/m ³	7900 kg/m ³
	thermal conductivity (k)	121 W/m · K	16.3 W/m · K
Thermal properties	heat capacity (c_p)	875 J/kg · K	500 J/kg · K
	thermal diffusivity (α)	49.7×10^{-6} m ² /s	4.13×10^{-6} m ² /s
Boundary parameters	convection coefficient (h)	5.00 W/m ² · K	5.00 W/m ² · K
	heat flux (q)	22 kW/m ²	5.5 kW/m ²
Sample dimensions	length (L)	300 mm	300 mm
	width (a)	25.4 mm	25.4 mm
	thickness (b)	6.35 mm	6.35 mm

Figure 4-1 presents the temperature change along the length of rectangular (a) aluminum and (b) stainless-steel alloys at different timeframes. The solid lines represent the 1D theoretically estimated temperature change, while the empty markers represent the corresponding 3D FEA simulated temperature change using COMSOL. In both cases,

the induced heat flux q values listed in Table 4-1 were selected to achieve an approximately 25 K maximum temperature change in both aluminum and stainless-steel samples at 360 s and 1800 s, respectively. The 5 frames displayed in Figure 4-1(a)–(b) for Al-2024 and SS-304 samples, respectively, were used to estimate the thermal diffusivity estimation of both materials. It should be noted that after conducting the 3D FEA, the heat diffusion experienced by the front surface of both materials were extracted and averaged along the y dimension to attain a 1D temperature change along the length of the samples.

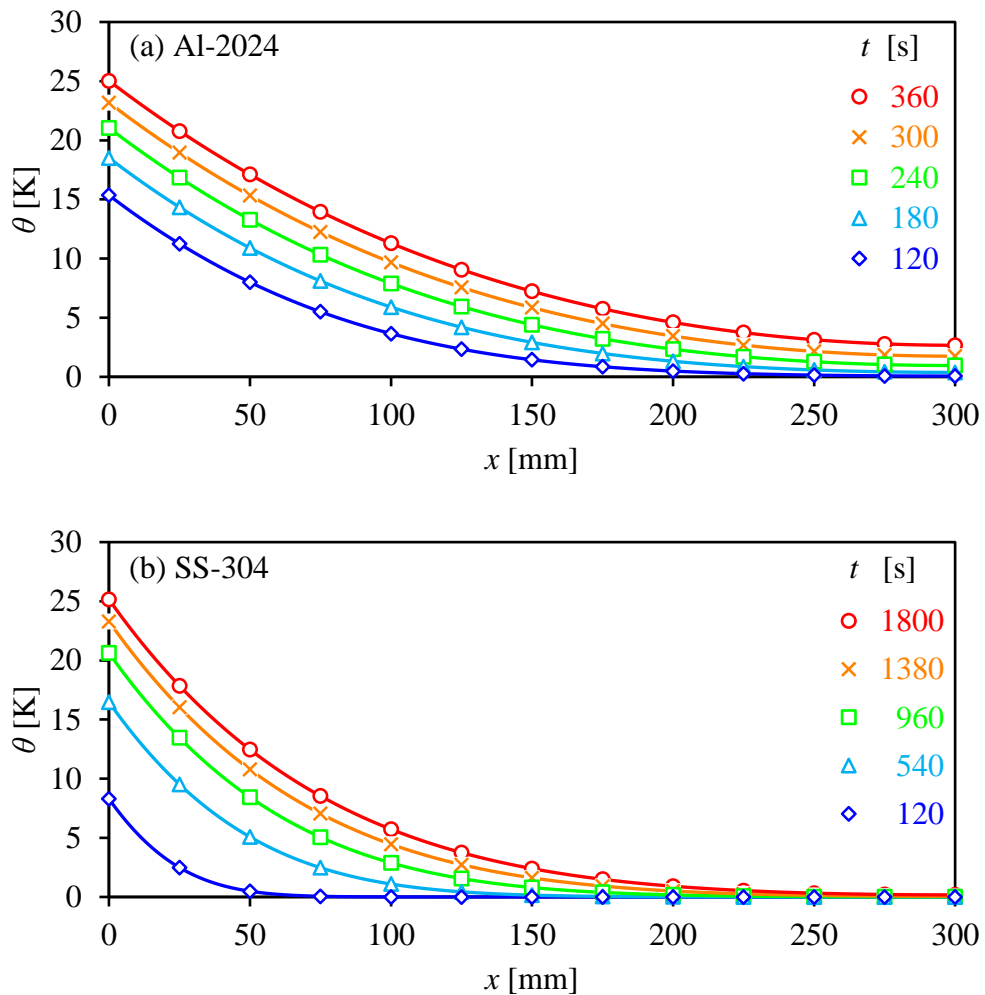


Figure 4-1: Estimated temperature change at different timeframes using the theoretical model (solid lines) and FE simulations (empty markers) over (a) Al-2024 and (b) SS-304 samples.

Apart from having a method that accurately estimates the thermal diffusivity of the samples being studied, the computational time it takes for the theoretical solution to

converge is equally important. The computational time in this method directly depends on how many N terms are used in Eq. (18). To properly determine the number of terms needed in the analysis, the 1D theoretical temperature change was conducted for values of N ranging from a single term $N = 1$ to $N = 100$. Then, the root mean square error (RMSE) was calculated by comparing the simulated temperature change at any N to the one estimated using $N = 100$. Finally, the RMSE for both samples was plotted against the number of terms (N) as shown through Figure 4-2. It could be seen that both samples have an RMSE value of less than 0.070 K when only 10 terms are used, which is sufficient for reaching an accurate estimation in this analysis and used in this study moving forward.

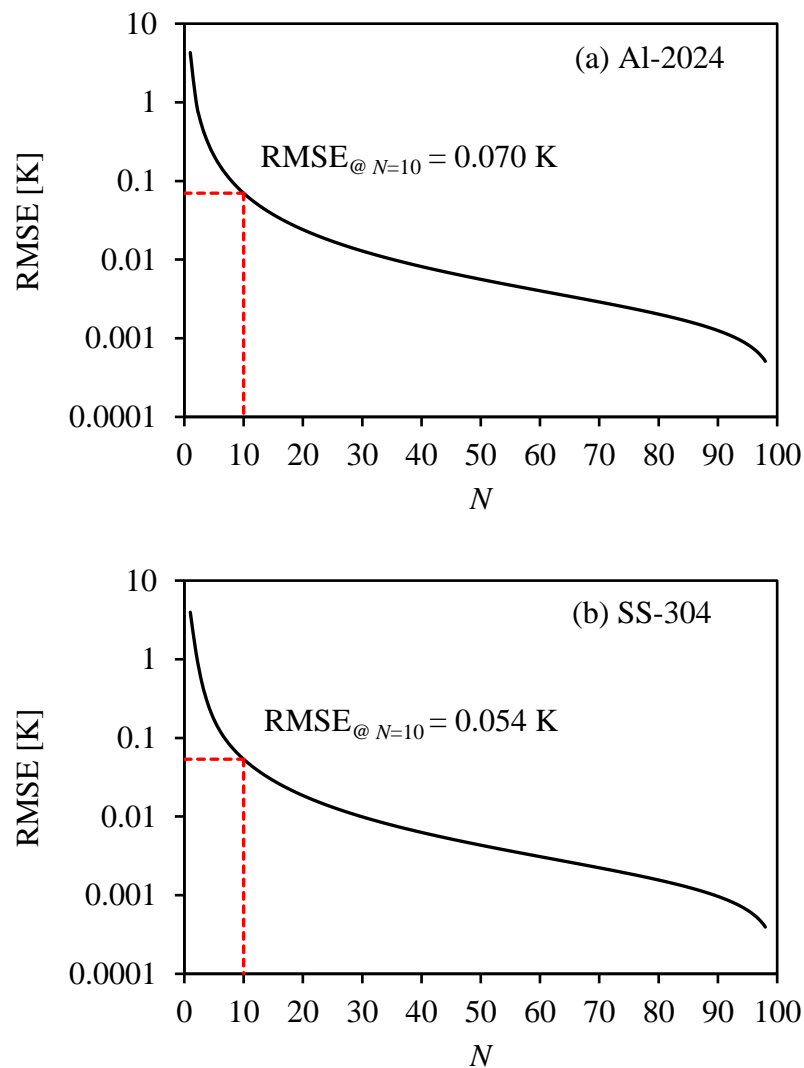


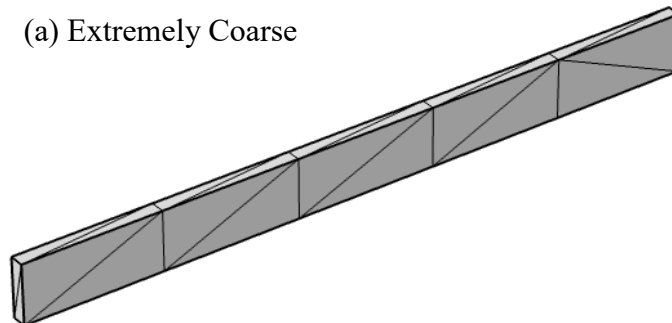
Figure 4-2: *RMSE* trend of theoretically estimated temperature change using different N number of terms ranging between 1 and 100 over (a) Al-2024 and (b) SS-304 samples.

4.2. FEA Mesh Independence

To validate the accuracy of the 3D FEA simulated temperature change along the sample's length conducted in COMSOL; it is important to conduct a mesh independence study and plot the obtained FEA simulated temperature change along with the 1D theoretically estimated temperature change obtained from Eqs. (15-18) using MATLAB. To do so, four different mesh sizes have been implemented to simulate the temperature change along one of the samples, the Al-2024 material, using COMSOL software. The mesh sizes selected are either extremely coarse, coarse, fine, or extremely fine as shown from Figure 4-3(a)–(d).

After changing the mesh sizes and conducting the FEA simulation, the simulated temperature change along the sample's length was plotted against the 1D theoretically estimated temperature change obtained from Eqs. (15-18) and discussed in Section 3.1. Figure 4-4(a)–(d) represent the obtained simulated temperature change along the sample's length through the different mesh sizes, respectively. The solid lines represent the 1D theoretically estimated temperature change while the empty markers represent the simulated FEA temperature change on COMSOL. It could be seen from Figure 4-4(a) and Figure 4-4(d), the simulated temperature change closely follows the ones estimated from the theoretical model, showing that using an extremely coarse mesh size will still provide accurate simulation. However, to reduce the need for investigating the mesh sizes through performing a mesh independence study on a case-to-case basis, the extremely fine mesh size represented in Figure 4-3(d) has been selected and implemented in this work.

(a) Extremely Coarse



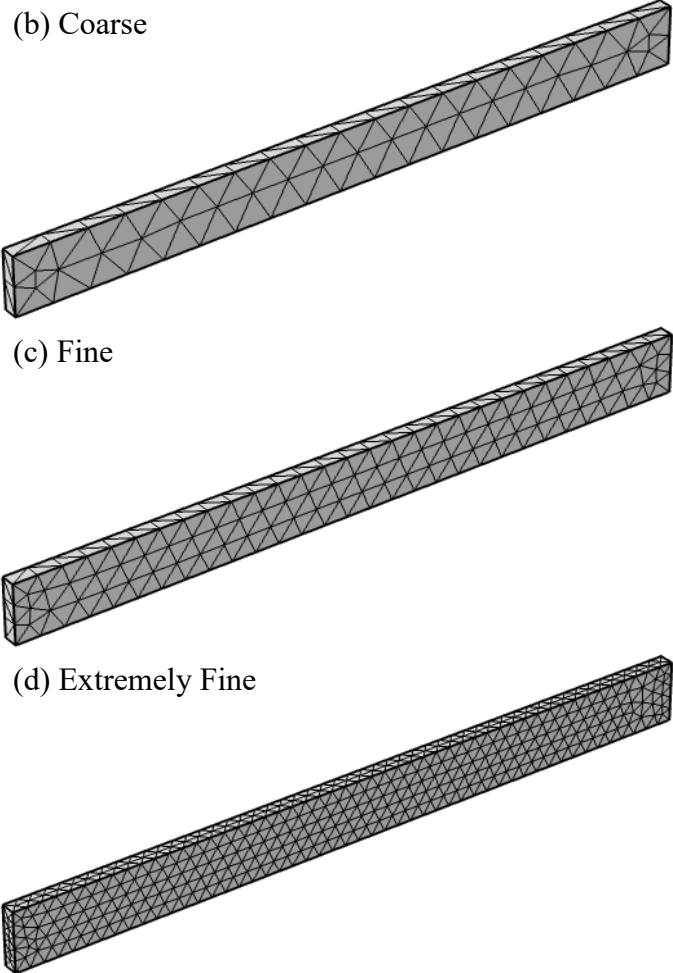
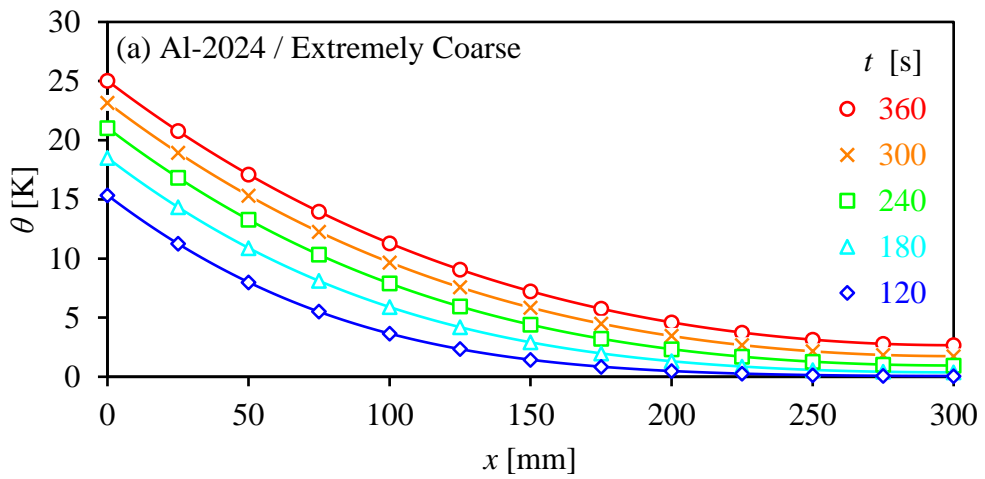


Figure 4-3: Schematic representation of the mesh independence study of the 3D FEA COMSOL simulation of the Al-2024 sample showing (a) extremely coarse, (b) coarse, (c) fine, and (d) extremely fine mesh sizes.



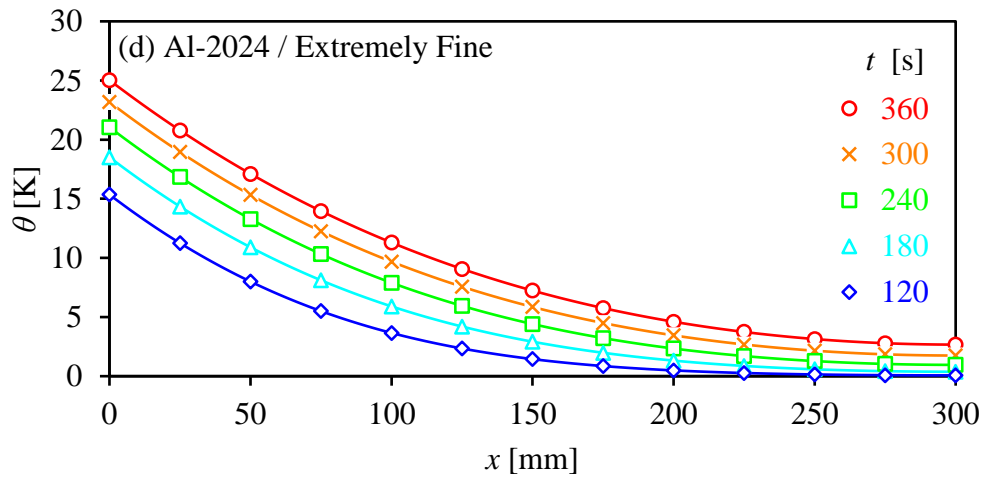
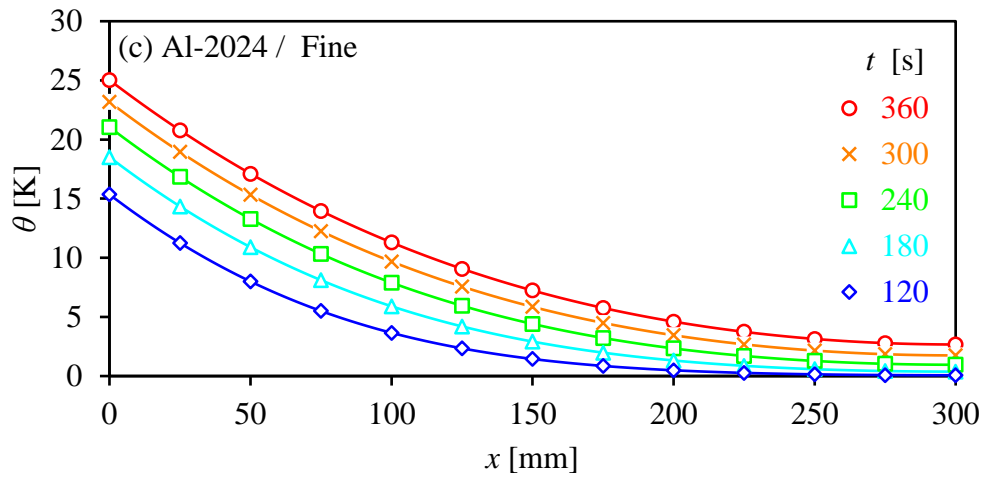
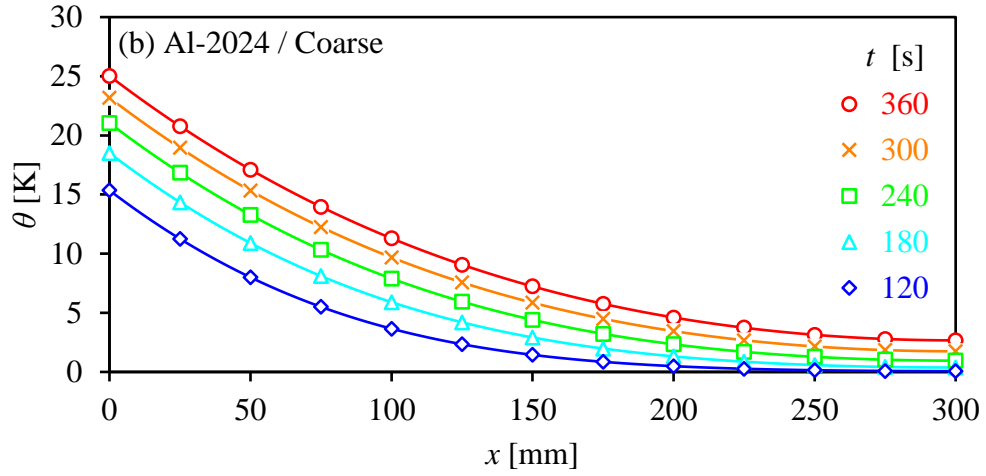


Figure 4-4: Estimated temperature change at different timeframes using the theoretical model (solid lines) and FE simulations (empty markers) over Al-2024 using (a) extremely coarse, (b) coarse, (c) fine, and (d) extremely fine mesh sizes.

4.3. Validation of Thermal Diffusivity Estimation

This section aims at estimating the thermal diffusivity (α) of both samples using COMSOL simulated data in Figure 4-1. It demonstrates the capability in retrieving the input thermal diffusivity (α_{in}) of the tested material and its boundary conditions, namely the input heat flux (q_{in}) and Biot number (Bi_{in}). An initial guess vector is assumed to start the optimization approach over several iterations using the following initial guesses of $q|_{i=0} = 5.65 \text{ kW/m}^2$, $Bi|_{i=0} = 0.01$ and $\alpha|_{i=0} = 50 \times 10^{-6} \text{ m}^2/\text{s}$ for the Al-2024 sample, and $q|_{i=0} = 2.17 \text{ kW/m}^2$, $Bi|_{i=0} = 0.1$ and $\alpha|_{i=0} = 4.0 \times 10^{-6} \text{ m}^2/\text{s}$ for the SS-304 sample. The initial guess is indicated by setting the iteration number i to zero. The convergence of the estimated induced heat flux (q_{est}), Biot number (Bi_{est}), thermal diffusivity (α_{est}) and error in thermal diffusivity estimates with iterations (i) is presented in Figure 4-5(a)–(d) for the Al-2024 sample and Figure 4-6(a)–(d) for the SS-304 sample. The method was not only able to precisely estimate the induced heat flux and Biot number experienced by both samples, but was also able to accurately retrieve the thermal diffusivities of both materials up to three significant digits. This illustrates the benefits of the presented 1D approach in estimating a material thermal diffusivity without the need to operate in a vacuum environment. It takes into account the convection heat loss without the need to ignore, assume or independently estimate the experienced Biot number of the sample with the surrounding environment. Moreover, it eliminates the need to control the input heat flux to a specific value as a predetermined boundary condition since it is also estimated using the proposed approach.

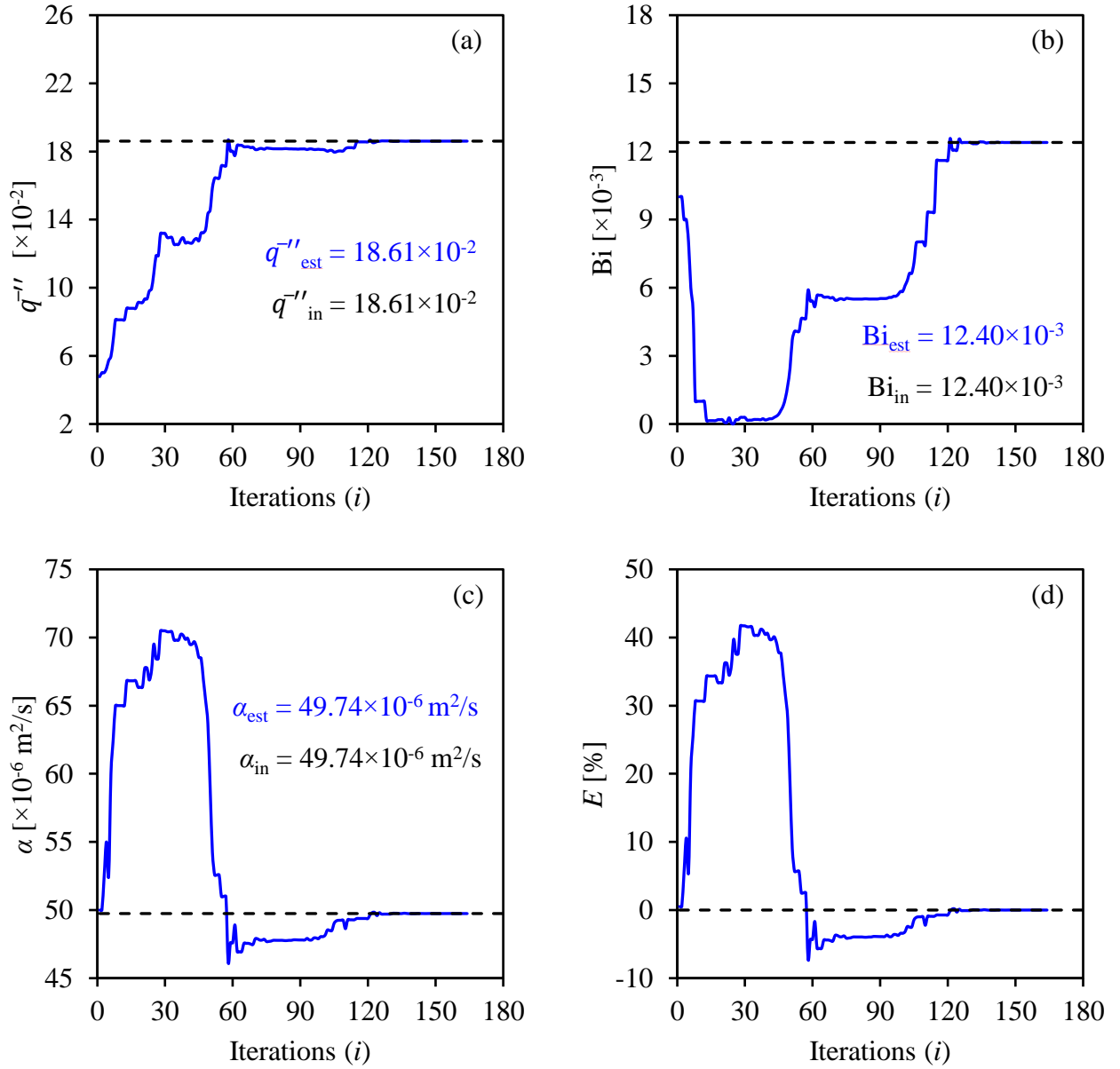


Figure 4-5: The convergence of estimated (a) dimensionless heat flux, (b) Biot number, (c) thermal diffusivity and (d) error in thermal diffusivity estimation with iterations using Al-2024 FE simulated data.

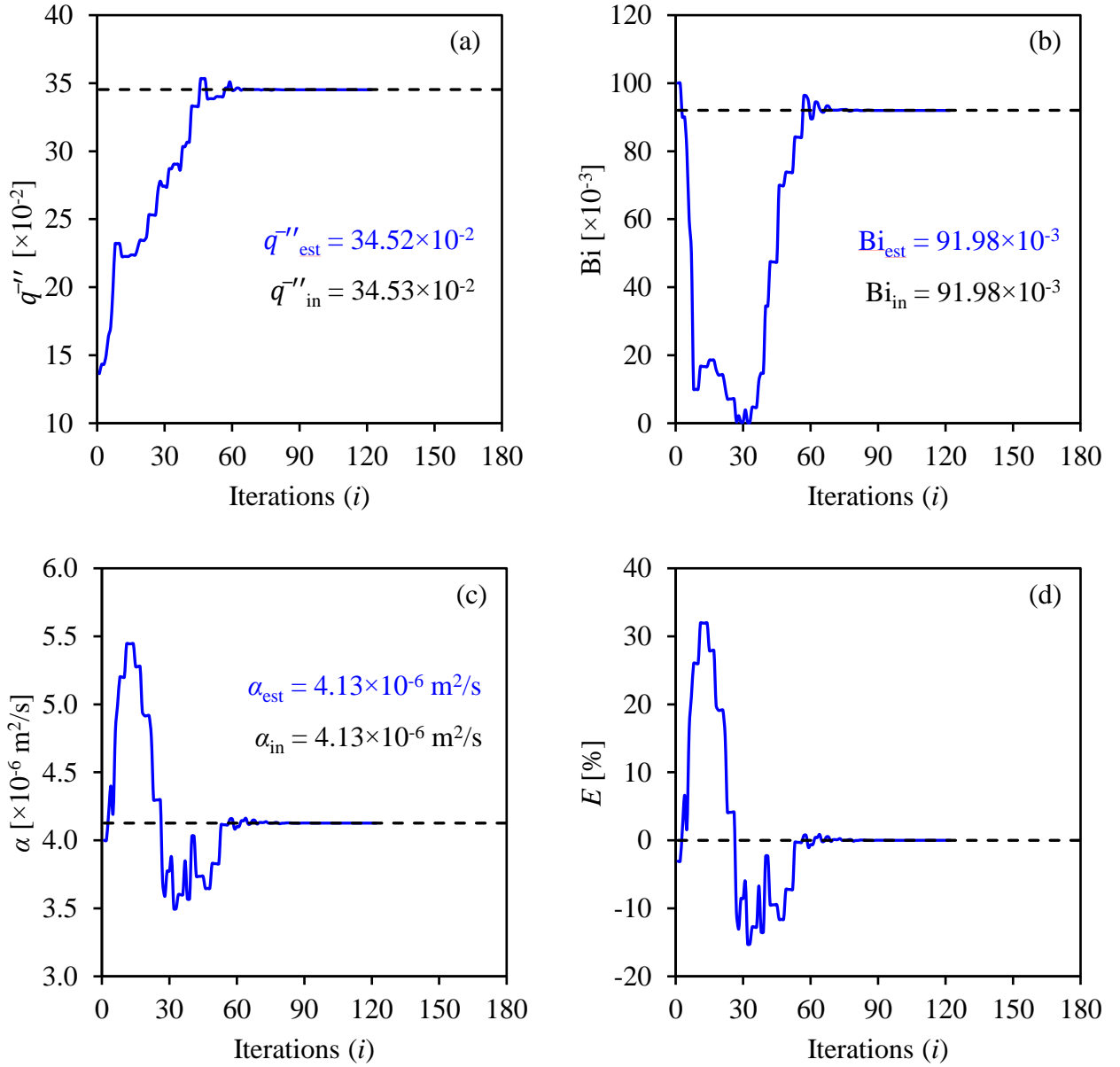


Figure 4-6: The convergence of estimated (a) dimensionless heat flux, (b) Biot number, (c) thermal diffusivity and (d) error in thermal diffusivity estimation with iterations using SS-304 FE simulated data.

To further validate the adequacy of using $N = 10$ terms in estimating a material thermal diffusivity, three realistic random noise levels of 30 mK increments were separately added to COMSOL simulated temperature change. The 30 mK random noise level was selected in agreement with the sensitivity of the IR camera used in this study. The percentage uncertainty in the estimated thermal diffusivities with the number of terms (N) is presented in Figure 4-7 for both (a) Al-2024 and (b) SS-304. The number of N terms needed to accurately estimate the material thermal diffusivity within a 0.1% error

is 3 for Al-2024 and 6 for SS-304. It is evident from the trend experienced in both materials that using $N > 6$ results in a negligible error in estimated thermal diffusivity values of both materials. To reduce the need for investigating the number of N terms needed on a case-to-case basis, a high enough number should be selected to reach accurate thermal diffusivity estimation while being not computationally expensive. Thus, the use of only 10 terms in the analysis is indeed sufficient in reporting accurate estimates, even at a high noise level of 90 mK, verifying the adequacy of the approach taken in this study. This is mainly due to the large number of thermal data points used in fitting or estimating a material thermal diffusivity and the targeting of a high signal-to-noise ratio when a peak temperature change of 25 K is reached to reduce the inversion sensitivity to the added noise.

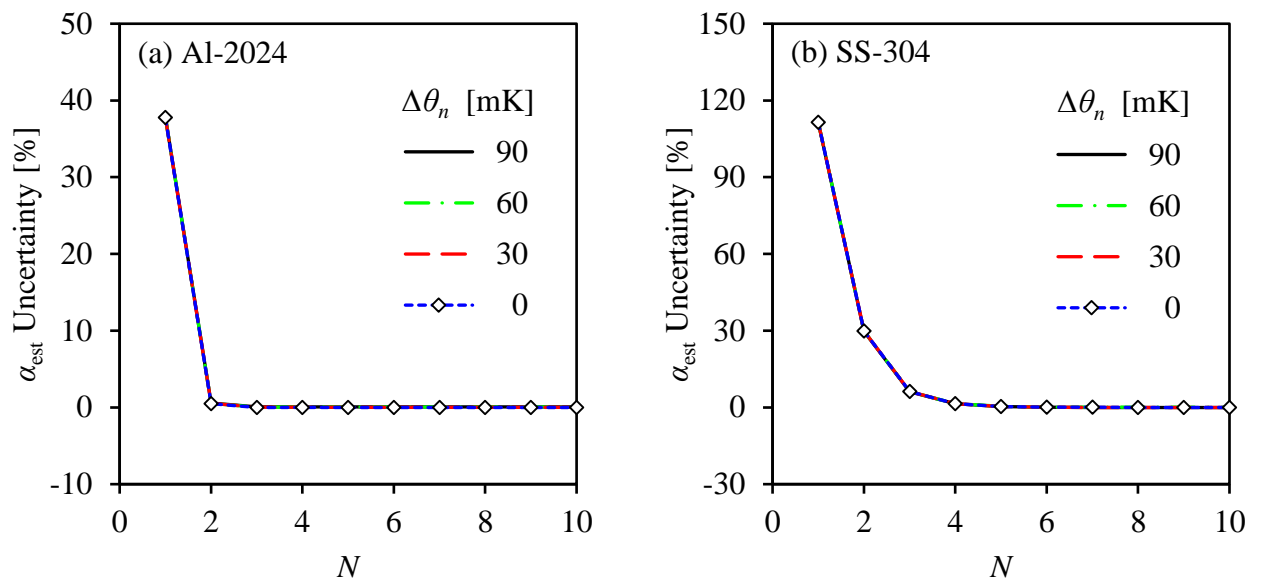


Figure 4-7: The criteria for selecting the least N number of terms needed to reduce the thermal noise $\Delta\theta_n$ effect in thermal diffusivity estimation over FE simulated thermal data for (a) Al-2024 and (b) SS-304.

Chapter 5. Experimental Setup

This section of the paper addresses the sample design, the emissivity check, the thermography setup, and the experimental procedure used in this study. The left side of the sample is excited with a steady heat flux source using a strip heater while an IR camera monitors the front side of the sample.

5.1. Sample Design

The thermal diffusivity estimation approach has been tested over two different alloys, namely tempered aluminum (Al-2024 T4) and annealed stainless-steel (SS-304) alloys. The aluminum alloy will be referred to as Al-2024 while the annealed stainless-steel alloy will be referred to as SS-304. Al-2024 is the main concern behind this study as it is extensively used in the aerospace industry. To mitigate being restrained towards thermally characterizing highly conductive materials such as Al-2024, the method is validated by a much lower thermally diffusive and extremely common metallic material, namely SS-304. A bar from each material was cut into a rectangular specimen that is 300 mm long \times 25.4 mm wide \times 6.35 mm thick in agreement with the samples dimensions used in the 3D FEA. All physical and thermal properties of the samples along with their dimensions are listed in Table 4-1.

The surfaces of tested alloys have low emissivity values. The front surface of each sample was coated using a black Plasti Dip coating, which can be easily peeled off when needed leaving no traces on the surfaces behind. Furthermore, a Plexiglas fixture was manufactured using a laser cutter to guarantee that the samples are perfectly oriented relative to the camera, mimicking the use of precision-positioning equipment in the aviation industry where precision is of utmost importance. Moreover, the fixture was designed using only two contact positions to allow minimum contact with the samples and provide stable positioning while ensuring that convection takes effect from the samples' exposed surfaces as proposed in the model and displayed in Figure 3-1.

5.2. Emissivity Check

For objects to be visible and distinct in a thermal image, the infrared radiation collected by the IR camera from the objects in the scene should be different [54]. The infrared signature of an object depends on its temperature distribution and emissivity of its material/s [55]. Emissivity (ϵ) of a material, is a dimensionless coefficient ranging from 0 to 1 indicating the object's ability to emit infrared radiation in comparison to a

blackbody at the same temperature. A blackbody is a theoretical material with $\varepsilon = 1$, meaning that it absorbs and perfectly re-emits all incident infrared radiation [56]. Therefore, an object with an emissivity value close to zero, emits a fraction of the thermal radiation radiated by an object with an emissivity value close to one. The emissivity of an object depends on many parameters, these include: the material, structure, and texture of an object's surface, the surface temperature of the object, and the wavelength of the thermal radiation collected by the IR camera [57], [58]. Thus, the emissivity coefficient (ε) is the ratio of the thermal radiation emitted by the imaged object $M(T)$ to the thermal radiation emitted by the blackbody $M_0(T)$ at identical thermal conditions [59], as follows:

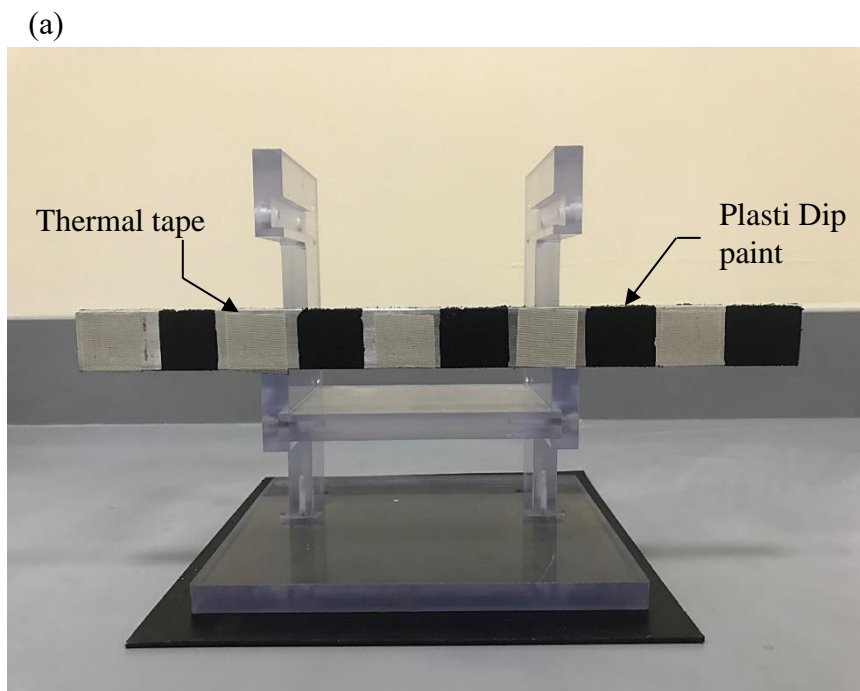
$$\varepsilon = \frac{M(T)}{M_0(T)} \quad (21)$$

Moreover, one particular case where the emissivity of the surface does not influence the contactless measurement of the surface temperature, as emitted or reflected infrared radiation becomes independent of the object's surface emissivity; is when the environmental/background temperature is identical to the objects temperature [54], causing the target to be indistinguishable in a thermal image. The solution to this issue is to heat the object or place it in an environment having a different background temperature. This is not a concern in this study, as the sample is already being heated using a constant heat flux-based system which raises the temperature of the sample considerably compared to the background environmental temperature.

The American Society for Testing and Materials (ASTM) define two standard test methods for determining the emissivity of objects when measuring their surface temperatures using infrared imaging radiometers [60]. The first method, called the Contact Thermometer Method (CTM), involves the use of contact thermometer to measure the temperature of a point or area where the emissivity is to be defined; the emissivity on the infrared imaging radiometer or IR camera's computer, focused on the same spot, is adjusted until both readings match. The second technique, called the Noncontact Thermometer Method (NTM), employs a surface-modifying material (SMM) of known emissivity and adhered to the target's surface, the IR camera's emissivity is set to the SMM value and the temperature value is recorded. Then the IR camera is focused on a spot on the target adjacent to the SMM where emissivity is to

be defined, and the IR camera's emissivity is adjusted until the temperature reading of this spot matches the one recorded on the SMM. Both methods require a minimum of three repetitions and the material's emissivity is the average of these repetitions.

This work followed the standard NTM to estimate the emissivity of the black Plasti Dip rubber coating discussed earlier in Section 5.1, with a thermal emission tape as the SMM. The thermal emission tape, manufactured by Testo SE & Co., has an emissivity of $\varepsilon = 0.95$ and temperature resistance of up to $+250\text{ }^{\circ}\text{C}$. Five locations have been selected to measure the emissivity of the coating as shown in Figure 5-1(a)–(b), to assure certainty. After adhering the SMM, the sample was left for few minutes to settle and reach a constant temperature, then thermal imaging was performed indoors. The emissivity check has been repeated ten times, meeting and exceeding the three repetition requirement set by the ASTM standard, with the average emissivity values of the five coatings over the ten repetitions being reported in Table 5-1. From the performed examination, the emissivity of this rubber-coated surfaces reported to be $\varepsilon = 0.909$. Moreover, it is recommended, when Plasti Dip rubber coating is used to enhance the emissivity of reflective surfaces, to apply two coats and ensure the coating thickness is less than $1/32''$ or 0.80 mm [61]. It should be noted that the rubber coating applied on the samples in this study satisfy these requirements.



(b)

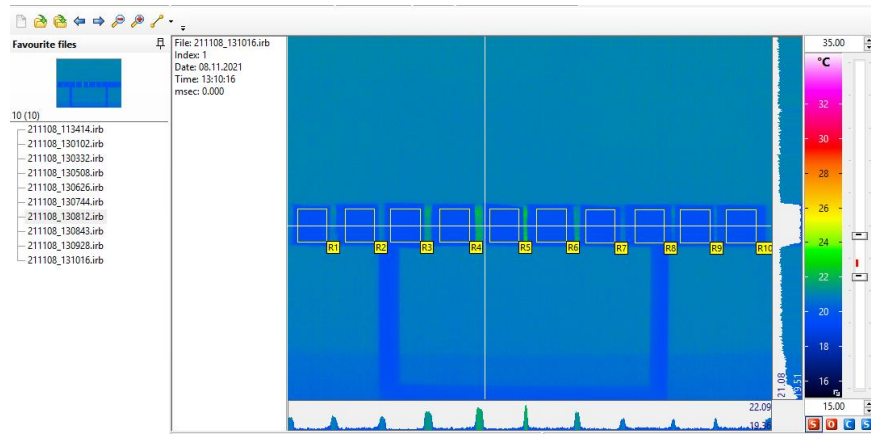


Figure 5-1: Emissivity check of the Plasti Dip black rubber coating using a thermal tape on five different locations shown by (a) the visible image and (b) the thermal image

Table 5-1: Reported emissivity values of the rubber coating over 10 repetitions.

Repetitions	1	2	3	4	5	6	7	8	9	10
ϵ	0.899	0.908	0.909	0.910	0.910	0.910	0.910	0.911	0.912	0.913
ϵ_{avg}	0.909									

5.3. Thermography System

The thermography setup used in this study is displayed in Figure 5-2(a) where the system consists of an Aim-TTi CPX400A DC bench power supply unit which can supply up to 60 V and 20 A of direct current. This DC bench power supply is connected to a 12 V 12 W flexible polyimide film heater that is 10 mm wide and 93 mm long. The film heater, which is manufactured by Icstation, is fixed to the left end of the sample positioned on the Plexiglas fixture. As shown from Figure 5-2(b), the strip heater consists of a flexible polyimide film with a thermo foil that comes into contact with the sample's left end using a 3M™ thermal self-adhesive. InfraTec VarioCAM HD Head-600 IR camera with a resolution of 480×640 pixels along with a temperature sensitivity of 0.03 K and up to 60 Hz or 60 frames per second acquisition rate is utilized to record the temperature profile of the samples with time as they are heated. Lastly, a laptop is used to operate the acquisition process by controlling the IR camera's parameters through InfraTec's IRBIS 3 plus thermography analysis software.

After ensuring that the samples are perfectly horizontal as discussed in Section 5.1, the IR camera is positioned and focused on the samples such that their entire length almost

encompasses the 640 pixel frame length. Using a measuring box in the software, the thermal image of the sample was manually enclosed in a rectangular frame that has an average size of 615×45 pixels. The rectangular frame pixel resolution is quantified in each run. This rectangular frame is used to export the raw temperature readings of the samples as they are being heated with time. Based on the experimental analyses done, a heating period of 1800 s was selected to allow heat to diffuse and reach the right end of both samples and a 2 Hz acquisition framerate was chosen. All parameters used in this experimental system are listed in Table 5-2.

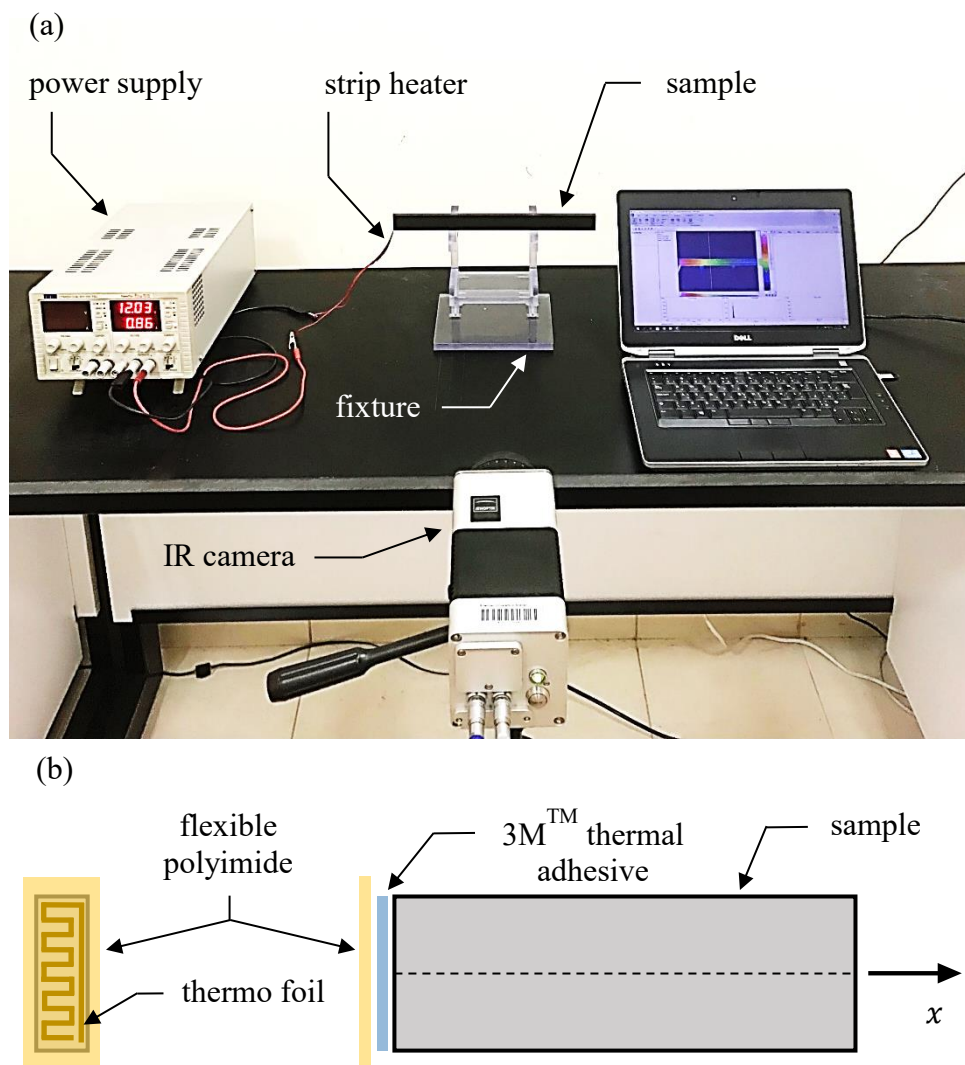


Figure 5-2: A presentation of (a) the experimental setup used in this study and (b) the strip heater in contact with the sample's left side.

Table 5-2: Thermography setup parameters.

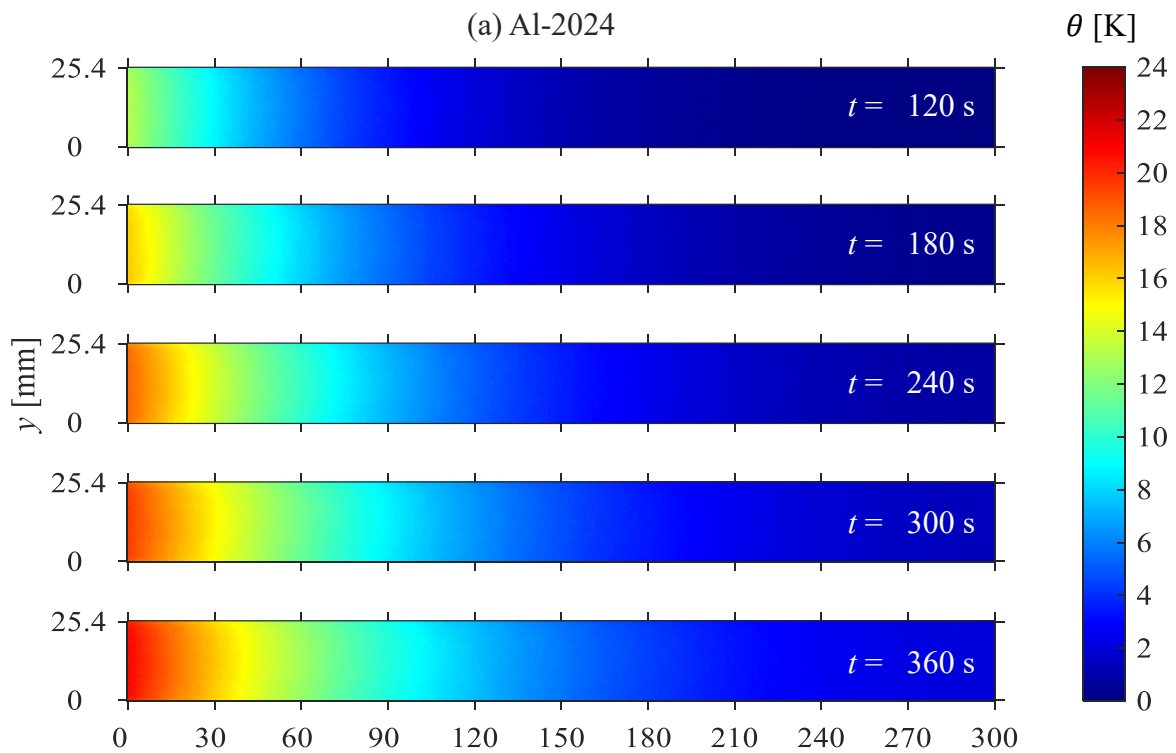
	Parameters	Value
IR camera	heating period	1800 s
	framerate	2 frames per second
	emissivity (ϵ)	0.909
	thermal image resolution	615×45 pixels

5.4. Experimental Procedure

Before switching on the power supply unit, the IR camera starts recording for 20 s at a 6 Hz frame rate, resulting in approximately 120 frames of temperature readings to estimate the reference temperature of the sample before excitation (T_0). The frame acquisition rate is then reduced to 2 frames per second and the power supply unit is switched on to start inducing heat into the samples simultaneously. The excitation period was stopped upon reaching a temperature change of ≈ 22 K on the left end of the sample. Non-uniformity of an IR camera's sensors due to minor detector drifts result in slowly-varying structured spatial row or line noise patterns imposed on the infrared image [62], [63]. This non-uniformity noise or fixed pattern noise is mainly due to the change in scenes and the IR camera's own radiation which affects both image quality and temperature readings. This non-uniformity is amplified in uncooled infrared cameras, such as the one used in this study, where it has been shown that some uncooled cameras require a correction every 30 s [63]. There are many non-uniformity correction (NUC) algorithms that have been developed for different applications to ensure highest image quality. In this study, a built-in NUC option in the IR camera's IRBIS software is utilized and set for correction every 30 s.

After the end of the excitation period, the recording is stopped and the power unit is switched off while the created rectangular frame bracketing the sample allow exporting of the sample's raw temperature readings only and not the entire field of view (FOV). To create the temperature difference readings, the unheated 120 frames are averaged across the 20 s resulting in a single 2D temperature reading representing the initial temperature (T_0) of the samples before switching the heater on. This averaged initial temperature reading is then subtracted from the temperature measurements of the

heated sample forming the temperature change $\theta(x, y, t)$ shown in Figure 5-3 for both tested alloys at the selected time frames from the start of the excitation period. Figure 5-3(a) shows the temperature change in the Al-2024 alloy of high thermal diffusivity and Figure 5-3(b) shows the temperature change in the SS-304 alloy of low thermal diffusivity. The input heat flux used on the left side of the SS-304 rectangular sample is approximately 4 times lower than that used over the Al-2024 sample in agreement with the simulation values shown in Table 4-1. This allows for the heat to diffuse enough through the SS-304 sample before reaching the peak temperature change of ≈ 22 K and offers a better utilization of the sample length in retrieving the material thermal diffusivity.



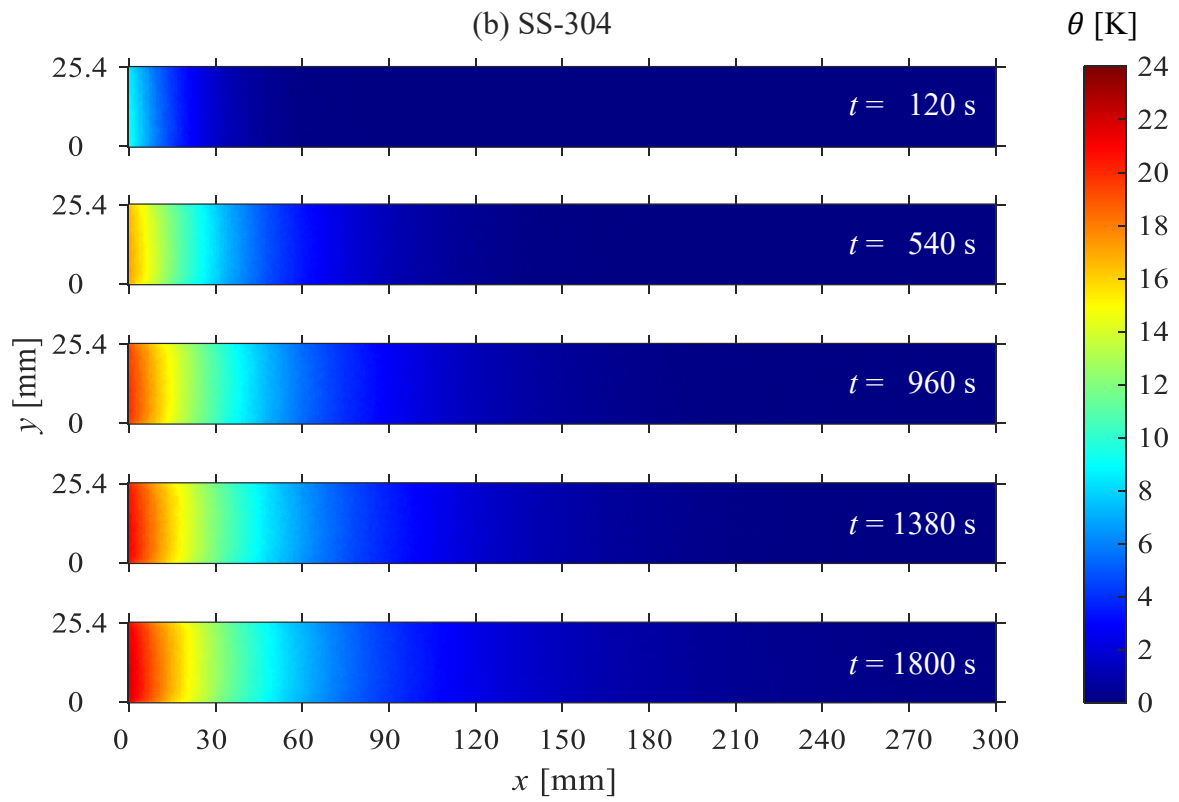


Figure 5-3: Thermal images $\theta(x, y, t)$ captured at different timeframes for (a) Al-2024 and (b) SS-304 samples.

Chapter 6. Results and Discussion

As mentioned above in the previous section, Figure 5-3 displays the temperature change $\theta(x, y, t)$ for both alloys as they are being heated from the left end of the samples. Figure 5-3(a) represents the temperature change through time along the Al-2024 alloy where it could be seen that the sample takes 360 s to reach a peak temperature change of ≈ 22 K, and the rightmost end of the sample shows a temperature change of ≈ 5 K. Contrarily, Figure 5-3(b) displays the temperature change through time along the SS-304 alloy where it could be seen that the stainless-steel alloy sample took 1800 s to reach a peak temperature change of ≈ 22 K, as endured by the aluminum sample, while the peak temperature change at the rightmost end of the sample is ≈ 1 K. This indicates that for a given excitation, Al-2024 conducts the imposed heat better and faster than the SS-304 alloy. Hence, this proves that the Al-2024 alloy has higher thermal conductivity and diffusivity when compared to the SS-304 alloy as expected, where the theoretical values of the thermal conductivity and diffusivity of Al-2024 listed in Table 4-1 show a one-order of magnitude higher than that for SS-304.

As the proposed method utilizes a 1D transient temperature change to estimate a material's thermal diffusivity, the measured temperature change $\theta(x, y, t)$ was averaged along the y dimension resulting in a 1D transient temperature change $\theta(x, t)$ along the sample length. Plots of these experimental temperature change (θ) variations in both materials are presented in Figure 6-1 for the selected time frames. The solid lines represent the theoretical 1D transient temperature change $\theta(x, t)$ along the sample from estimated V parameters while the solid markers represent the experimental thermal measurements obtained by the IR camera. Figure 6-1(a)–(b) presents 5 frames of the temperature change along the length of the Al-2024 and the SS-304 samples through the selected time periods, respectively. Thermal measurements were used at a rate of 1 frame per second starting at 120 s up to 360 s for Al-2024 and up to 1800 s for SS-304 to experimentally estimate their thermal diffusivity values.

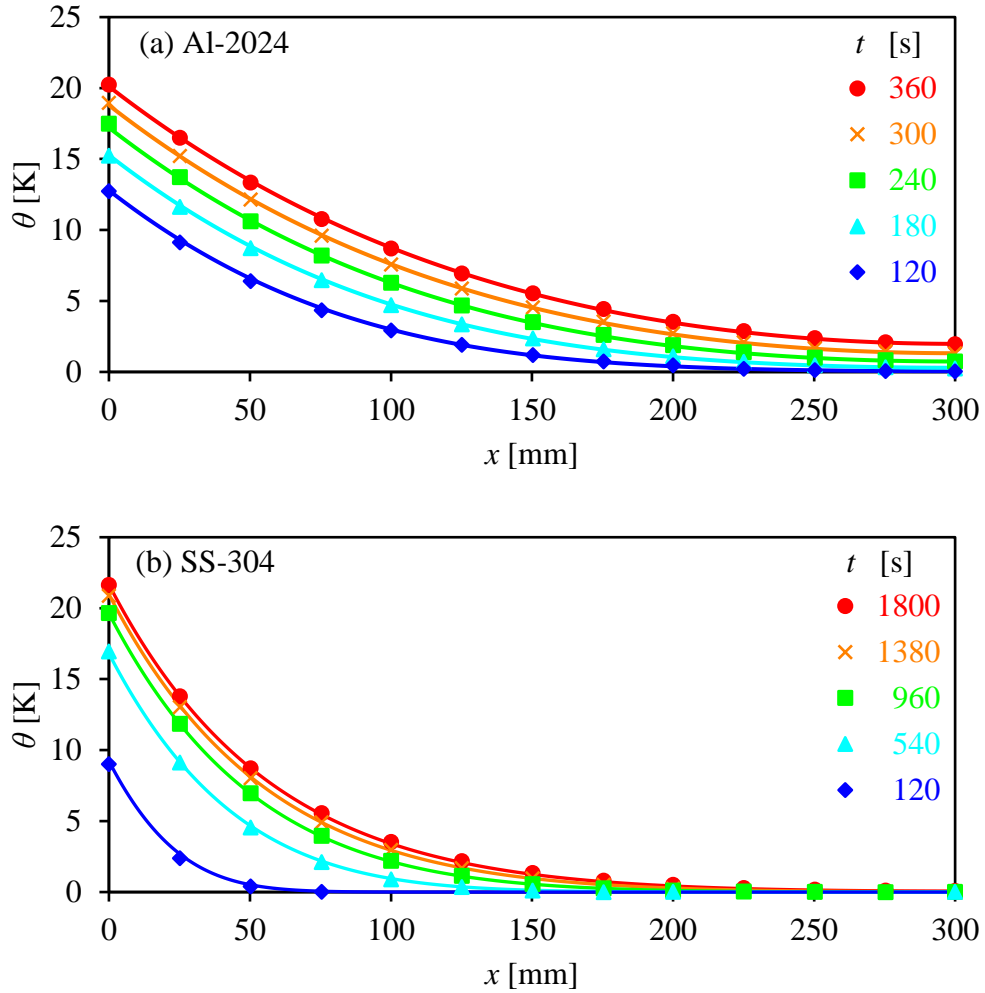


Figure 6-1: Average temperature change $\theta(x, t)$ at different timeframes using the theoretical model (solid lines) and experimental data (solid markers) over (a) Al-2024 and (b) SS-304 samples.

It could be seen from Figure 6-1(a)–(b) that the temperature change readings obtained from the experimental trials using the IR camera, shown by the solid markers, closely follow the theoretical 1D temperature change, represented by the solid lines, obtained from the theoretical model discussed in Section 3.1. Observing the trend experienced by both materials, Al-2024 alloy show a flatter temperature distribution compared to the much steeper trend experienced by the SS-304 alloy. This indicates how the Al-2024 sample is more thermally conductive and diffusive than the SS-304. Furthermore, focusing on the peak temperature change reached by both materials, it could be seen that the Al-2024 alloy took 360 s to reach a peak temperature change of ≈ 22 K while the SS-304 alloy took 1800 s to reach approximately the same temperature reading.

This proves the deduction reached from Figure 5-3(a)–(b) mentioned earlier. Overall, seeing the experimental temperature change readings closely following the trends obtained from the theoretical model in Figure 6-1(a)–(b), indicates the accuracy of the 1D theoretical model and its use in estimating a metallic alloy thermal diffusivity as proposed in this study.

Similar to the analysis done in Section 4.2 using COMSOL simulated data, the uncertainty of experimentally estimated thermal diffusivity for both materials when compared to the reference values listed in Table 4-1 have been plotted against the number of N terms used in Eq. (18) and shown in Figure 6-2 for (a) Al-2024 and (b) SS-304 alloys. The experimental trend represented by Figure 6-2 closely follows the one obtained from the FEA represented by Figure 4-7 for both alloys. Likewise, a matching conclusion is reached, where it could be seen that using $N > 4$ results in a 0.07% and a -0.16% uncertainty in experimentally estimated thermal diffusivities of Al-2024 and SS-304, respectively. Furthermore, the experimentally estimated thermal diffusivity values with the number of iterations (i) is illustrated in Figure 6-3 for (a) Al-2024 and (b) SS-304 alloys. Figure 6-2 and Figure 6-3 display the outcome obtained by one of the nine trials taken on each material. The experimental trial has been repeated nine times on each sample, obtaining nine temperature readings for every alloy. Table 6-1 lists the experimental thermal diffusivity estimates of all nine trials along with their average uncertainties when compared to the reference values listed in Table 4-1. Notably, the average uncertainty of the nine thermal diffusivity estimates is 1.39% and -0.70% for Al-2024 and SS-304, respectively. This strongly supports the efficacy of the proposed approach in estimating the thermal diffusivity of both high and low thermal diffusivity alloys where the aluminum alloy has a one-order of magnitude higher thermal diffusivity than the stainless-steel alloy.

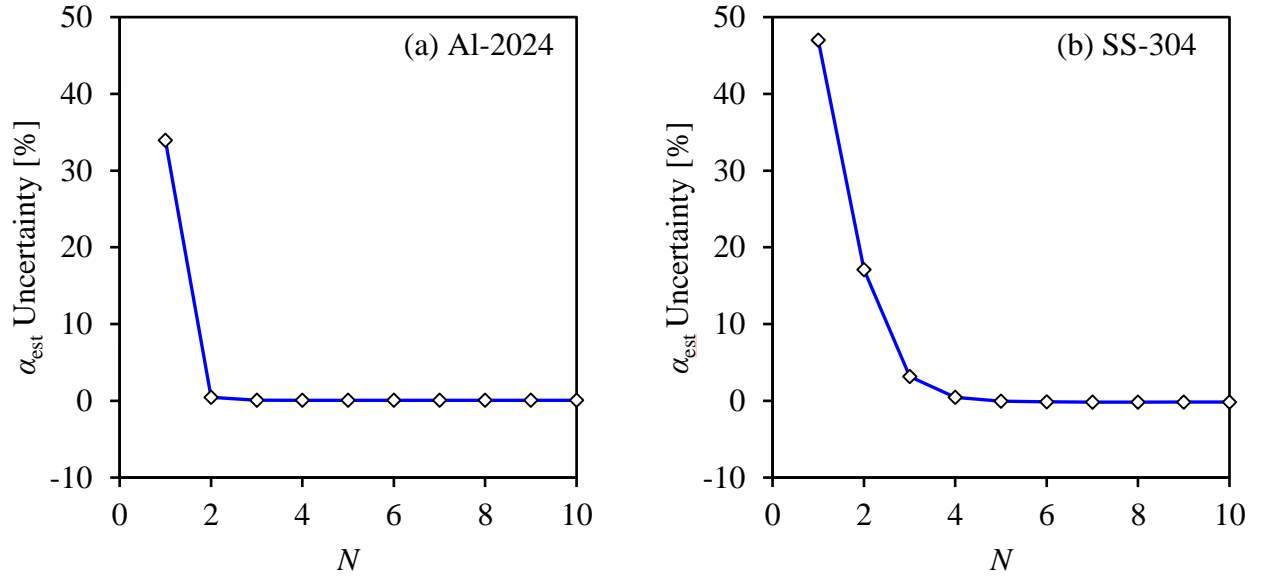


Figure 6-2: Experimental uncertainty in thermal diffusivity estimation of the (a) Al-2024 and (b) SS-304 samples using different N number of terms.

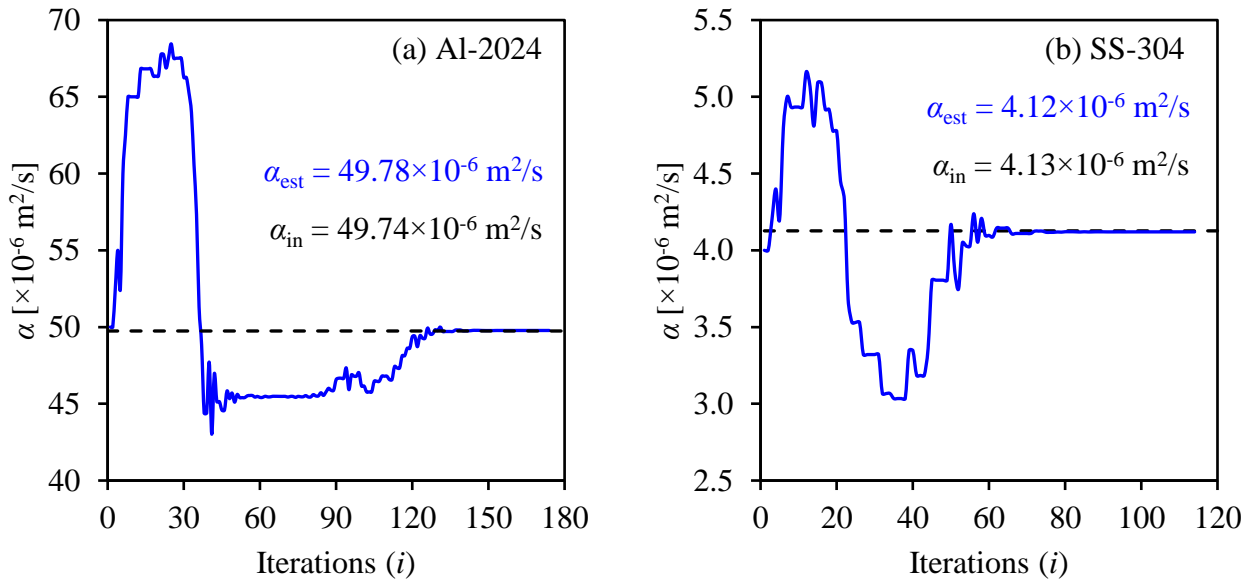


Figure 6-3: The convergence in experimental thermal diffusivity estimation of the (a) Al-2024 and (b) SS-304 samples with iterations.

Table 6-1: Summary of experimental thermal diffusivity estimates and their uncertainties.

	Al-2024		SS-304	
Trial #	α [$\times 10^{-6}$ m ² /s]	E [%]	α [$\times 10^{-6}$ m ² /s]	E [%]
1	50.1237	0.77	4.0618	-1.57
2	51.6667	3.87	4.1200	-0.16
3	51.0505	2.63	3.8844	-5.87
4	49.7755	0.07	4.1592	0.79
5	49.9968	0.45	4.1456	0.46
6	49.0796	-1.33	4.0556	-1.72
7	51.5964	3.73	4.2725	3.54
8	50.2698	1.06	4.0664	-1.46
9	50.3707	1.26	4.1146	-0.29
Reference	49.7431 [52]	–	4.1266 [53]	–
Mean	50.4366	1.39	4.0978	-0.70

Chapter 7. Summary and Future Work

7.1. Conclusion

This study targeted the development of a simple experimental thermography technique to accurately estimate a metallic alloy thermal diffusivity. The proposed 1D infrared thermography inspection technique is implemented by heating the metallic rectangular samples through a uniform flux-based excitation source. A theoretical model has been developed to account for the sample dimensions, material thermal properties, effective heat convection coefficient with the surrounding environment and a uniform heat flux applied to the sample. The effective convection heat transfer coefficient combines the natural convection and radiation endured by the sample to the surrounding environment. The proposed method successfully estimated the thermal diffusivity of two different alloys by employing the forward theoretical model of heat diffusion and the direct search method. It requires no information on the applied heat flux nor the effective convection heat transfer coefficient with the surrounding environment as the adopted approach is used to estimate the heat flux, Biot number, and the material thermal diffusivity of interest. It is demonstrated that the proposed method delivers an uncertainty of less than 2% in material thermal diffusivity estimation when tested experimentally over a high thermal diffusivity aerospace grade aluminum alloy (Al-2024 T4) and a one-order of magnitude lower thermal diffusivity in a stainless-steel alloy (SS-304). This makes the proposed 1D approximation method a practical, simple and accurate thermography technique for estimating thermal diffusivity of numerous alloys commonly used in the industry.

7.2. Future Work

The proposed 1D model is a robust and effective tool in estimating thermal diffusivity of high and medium conductivity metallic alloys while requiring no prior knowledge or specific control of experimental variables. Thus, future work could include the implementation of the proposed 1D model along with the optimization algorithm, to estimate material thermal diffusivity after removing the radial and tangential distortions caused by the IR camera's lens. Distortions caused by the curved nature of the camera's lens deform the captured thermal images by adding pincushion or barrel effects. Geometric calibration involves the imaging of a calibration target of well-known geometric features to determine the parameters of the camera and remove distortions in

the captured images [64]–[66]. As this work requires the geometrical information, exact length of the samples being thermally imaged, removing distortions through a simple geometric calibration to the IR camera then using the proposed 1D model to estimate material thermal diffusivity, might prove accurate and practical.

References

- [1] Y. A. ÇENGEL and A. J. GHAJAR, *Heat and Mass Transfer: Fundamentals & Applications*, 5th ed. New York: McGraw-Hill Education, 2015.
- [2] P. W. Nolte, T. Malvisalo, F. Wagner, and S. Schweizer, “Thermal diffusivity of metals determined by lock-in thermography,” *Quant. Infrared Thermogr. J.*, vol. 14, no. 2, pp. 218–225, 2017, doi: 10.1080/17686733.2017.1329777.
- [3] P. F. Qiu, S. Y. Zhang, S. Z. Wu, Z. J. Chen, Z. N. Zhang, and X. J. Shui, “Characterisation of thermal property of materials by infrared thermography,” *Nondestruct. Test. Eval.*, vol. 25, no. 1, pp. 91–98, 2010, doi: 10.1080/10589750903473633.
- [4] F. Cernuschi, P. G. Bison, A. Figari, S. Marinetti, and E. Grinzato, “Thermal diffusivity measurements by photothermal and thermographic techniques,” *Int. J. Thermophys.*, vol. 25, no. 2, pp. 439–457, 2004, doi: 10.1023/B:IJOT.0000028480.27206.cb.
- [5] K. Kobayasi, “Recent developments in measuring techniques for thermal conductivity and thermal diffusivity,” *JSME Int. Journal. Ser. B Fluids Therm. Eng.*, vol. 31, no. 1, pp. 1–8, 1988.
- [6] D. A. P. Reis, A. A. Couto, N. I. Domingues Jr., A. C. Hirschmann, S. Zepka, and C. de Moura Neto, “Effect of Artificial Aging on the Mechanical Properties of an Aerospace Aluminum Alloy 2024,” in *Diffusion in Solids and Liquids VII*, 2012, vol. 326, pp. 193–198, doi: 10.4028/www.scientific.net/DDF.326-328.193.
- [7] F. Ciampa, P. Mahmoodi, F. Pinto, and M. Meo, “Recent advances in active infrared thermography for non-destructive testing of aerospace components,” *Sensors (Switzerland)*, vol. 18, no. 2, pp. 1–37, 2018, doi: 10.3390/s18020609.
- [8] N. D. Alexopoulos and P. Papanikos, “Experimental and theoretical studies of corrosion-induced mechanical properties degradation of aircraft 2024 aluminum alloy,” *Mater. Sci. Eng. A*, vol. 498, no. 1–2, pp. 248–257, 2008, doi: 10.1016/j.msea.2008.08.024.
- [9] N. Barakat, J. Mortadha, A. Khan, B. A. Abu-Nabah, M. O. Hamdan, and S. M. Al-Said, “A one-dimensional approach towards edge crack detection and mapping using eddy current thermography,” *Sensors Actuators, A Phys.*, vol.

- 309, pp. 1–10, 2020, doi: 10.1016/j.sna.2020.111999.
- [10] B. A. Abu-Nabah, S. M. Al-Said, and R. Gouia-Zarrad, “A simple heat diffusion model to avoid singularity in estimating a crack length using sonic infrared inspection technology,” *Sensors Actuators, A Phys.*, vol. 293, pp. 77–86, Jul. 2019, doi: 10.1016/j.sna.2019.03.001.
- [11] S. M. Al-Said and B. A. Abu-Nabah, “A simple algorithm based on a 2D heat diffusion mathematical model to extract a surface crack length from a sonic IR thermal image alone,” *J. Nondestruct. Eval.*, vol. 40, no. 98, pp. 1–17, 2021, doi: 10.1007/s10921-021-00832-3.
- [12] B. A. Abu-Nabah and S. A. M. Al-Said, “Sonic IR crack size estimation using 2D heat diffusion model with arbitrary heat source function along the crack,” *Quant. Infrared Thermogr. J.*, vol. 15, no. 2, pp. 271–290, Jul. 2018, doi: 10.1080/17686733.2018.1463011.
- [13] V. Bhargava, B. A. Abu-Nabah, and M. Alkhader, “A theoretical approach towards the modeling of vibrothermography using finite element methods,” *Eur. J. Mech. A/Solids*, vol. 91, pp. 1–14, Jan. 2022, doi: 10.1016/j.euromechsol.2021.104389.
- [14] D. Zhao, X. Qian, X. Gu, S. A. Jajja, and R. Yang, “Measurement techniques for thermal conductivity and interfacial thermal conductance of bulk and thin film materials,” *J. Electron. Packag. Trans. ASME*, vol. 138, no. 4, pp. 1–64, 2016, doi: 10.1115/1.4034605.
- [15] A. L. Pope, B. Zawilski, and T. M. Tritt, “Description of removable sample mount apparatus for rapid thermal conductivity measurements,” *Cryogenics (Guildf)*, vol. 41, no. 10, pp. 725–731, 2001, doi: 10.1016/S0011-2275(01)00140-0.
- [16] T. M. Tritt and D. Weston, “Measurement Techniques and Considerations for Determining Thermal Conductivity of Bulk Materials,” in *Thermal Conductivity: Theory, Properties, and Applications*, T. M. Tritt, Ed. Boston, MA: Springer US, 2004, pp. 187–203.
- [17] D. R. Flynn, “Thermal Conductivity of Loose-Fill Materials by a Radial-Heat-Flow Method,” in *Compendium of Thermophysical Property Measurement Methods: Volume 2 Recommended Measurement Techniques and Practices*, K.

- D. Maglić, A. Cezairliyan, and V. E. Peletsky, Eds. Boston, MA: Springer US, 1992, pp. 33–75.
- [18] O. Maldonado, “Pulse method for simultaneous measurement of electric thermopower and heat conductivity at low temperatures,” *Cryogenics (Guildf)*., vol. 32, no. 10, pp. 908–912, 1992, doi: 10.1016/0011-2275(92)90358-h.
- [19] S. E. Gustafsson, “Transient plane source techniques for thermal conductivity and thermal diffusivity measurements of solid materials Transient diffusivity plane source techniques for thermal conductivity measurements of solid materials and thermal,” *Rev. Sci. Instrum.*, vol. 62, no. 3, pp. 797–804, 1991, doi: 10.1063/1.1142087.
- [20] F. Völklein, H. Reith, and A. Meier, “Measuring methods for the investigation of in-plane and cross-plane thermal conductivity of thin films,” *Phys. Status Solidi Appl. Mater. Sci.*, vol. 210, no. 1, pp. 106–118, 2013, doi: 10.1002/pssa.201228478.
- [21] D. G. Cahill, H. E. Fischer, T. Klitsner, E. T. Swartz, and R. O. Pohl, “Thermal conductivity of thin films: Measurements and understanding,” *J. Vac. Sci. Technol. A Vacuum, Surfaces, Film.*, vol. 7, no. 3, pp. 1259–1266, 1989, doi: 10.1116/1.576265.
- [22] D. G. Cahill, “Thermal conductivity measurement from 30 to 750 K: The 3ω method,” *Rev. Sci. Instrum.*, vol. 61, no. 2, pp. 802–808, 1990, doi: 10.1063/1.1141498.
- [23] W. Ben Larbi, M. Klein, A. Bendada, and X. Maldague, “Experimental Comparison of Lock-in and Pulsed Thermography for the Nondestructive Evaluation of Aerospace Materials,” *NDT.net*, no. 2009–11, pp. 1–9, 2009.
- [24] X. Maldague, *Theory and practice of infrared technology for nondestructive testing*, 1st ed. New York: Wiley–Interscience, 2001.
- [25] W. J. Parker, R. J. Jenkins, C. P. Butler, and G. L. Abbott, “Flash method of determining thermal diffusivity, heat capacity, and thermal conductivity,” *J. Appl. Phys.*, vol. 32, no. 9, pp. 1679–1684, 1961, doi: 10.1063/1.1728417.
- [26] I. Philippi, J. C. Batsale, D. Maillet, and A. Degiovanni, “Measurement of thermal diffusivities through processing of infrared images,” *Rev. Sci. Instrum.*, vol. 66, no. 1, pp. 182–192, 1995, doi: 10.1063/1.1146432.

- [27] P. Jena and R. Gupta, “Simultaneous estimation of multiple thermal properties using single-sided step heating thermography,” *Infrared Phys. Technol.*, vol. 115, pp. 2–14, Jun. 2021, doi: 10.1016/j.infrared.2021.103726.
- [28] S. Addepalli, Y. Zhao, J. A. Erkoyuncu, and R. Roy, “Quantifying uncertainty in pulsed thermographic inspection by analysing the thermal diffusivity measurements of metals and composites,” *Sensors*, vol. 21, no. 16, Aug. 2021, doi: 10.3390/s21165480.
- [29] L. Vozár and W. Hohenauer, “Uncertainty of thermal diffusivity measurements using the laser flash method,” *Int. J. Thermophys.*, vol. 26, no. 6, pp. 1899–1915, Nov. 2005, doi: 10.1007/s10765-005-8604-5.
- [30] B. Hay, J. R. Filtz, J. Hameury, and L. Rongione, “Uncertainty of thermal diffusivity measurements by laser flash method,” *Int. J. Thermophys.*, vol. 26, no. 6, pp. 1883–1898, Nov. 2005, doi: 10.1007/s10765-005-8603-6.
- [31] N. W. Pech-May, Á. Cifuentes, A. Mendioroz, A. Oleaga, and A. Salazar, “Simultaneous measurement of thermal diffusivity and effusivity of solids using the flash technique in the front-face configuration,” *Meas. Sci. Technol.*, vol. 26, no. 8, pp. 1–8, Aug. 2015, doi: 10.1088/0957-0233/26/8/085017.
- [32] A. Greppmair, N. Galfe, K. Amend, M. Stutzmann, and M. S. Brandt, “Thermal characterization of thin films via dynamic infrared thermography,” *Review of Scientific Instruments*, vol. 90, no. 4. American Institute of Physics Inc., pp. 1–11, Apr. 01, 2019, doi: 10.1063/1.5067400.
- [33] C. S. Welch, D. M. Heath, and W. P. Winfree, “Remote measurement of in-plane diffusivity components in plates,” *J. Appl. Phys.*, vol. 61, no. 3, pp. 895–898, 1987, doi: 10.1063/1.338140.
- [34] S. Pham Tu Quoc, G. Cheymol, and A. Semerok, “Phase lock-in thermography for metal walls characterization,” 2013, doi: 10.1109/ANIMMA.2013.6727993.
- [35] K. Mouhoubi, J. L. Bodnar, S. Ousseni, J. L. Nicolas, and D. Caron, “Local thermal characterization of metal sample by stimulated infra-red thermography,” *Mech. Ind.*, vol. 15, no. 4, pp. 307–312, 2014, doi: 10.1051/meca/2014037.
- [36] N. W. Pech-May, A. Mendioroz, and A. Salazar, “Simultaneous measurement of the in-plane and in-depth thermal diffusivity of solids using pulsed infrared thermography with focused illumination,” *NDT E Int.*, vol. 77, pp. 28–34, Jan.

- 2016, doi: 10.1016/j.ndteint.2015.10.001.
- [37] D. Moskal, J. Martan, V. Lang, M. Švantner, J. Skála, and J. Tesař, “Theory and verification of a method for parameter-free laser-flash diffusivity measurement of a single-side object,” *Int. J. Heat Mass Transf.*, vol. 102, pp. 574–584, Nov. 2016, doi: 10.1016/j.ijheatmasstransfer.2016.06.073.
- [38] A. Salazar, M. Colom, and A. Mendioroz, “Laser-spot step-heating thermography to measure the thermal diffusivity of solids,” *Int. J. Therm. Sci.*, vol. 170, pp. 1–8, Dec. 2021, doi: 10.1016/j.ijthermalsci.2021.107124.
- [39] P. G. Bison, E. Grinzato, and S. Marinetti, “Local thermal diffusivity measurement,” *Quant. Infrared Thermogr. J.*, vol. 1, no. 2, pp. 241–250, 2004, doi: 10.3166/qirt.1.241-250.
- [40] C. Pradere, L. Clerjaud, J. C. Batsale, and S. Dilhaire, “High speed heterodyne infrared thermography applied to thermal diffusivity identification,” *Rev. Sci. Instrum.*, vol. 82, no. 5, pp. 2–7, 2011, doi: 10.1063/1.3581335.
- [41] T. Yamane, S. I. Katayama, and M. Todoki, “Measurement of thermal diffusivity parallel to the surface of platelike specimen by the laser pulse heating method,” *Rev. Sci. Instrum.*, vol. 67, no. 12, pp. 4261–4267, 1996, doi: 10.1063/1.1147524.
- [42] M. A. Sheikh, S. C. Taylor, D. R. Hayhurst, and R. Taylor, “Measurement of thermal diffusivity of isotropic materials using a laser flash method and its validation by finite element analysis,” *J. Phys. D. Appl. Phys.*, vol. 33, no. 12, pp. 1536–1550, 2000, doi: 10.1088/0022-3727/33/12/316.
- [43] A. Mendioroz, R. Fuente-Dacal, E. Apianiz, and A. Salazar, “Thermal diffusivity measurements of thin plates and filaments using lock-in thermography,” *Rev. Sci. Instrum.*, vol. 80, no. 7, pp. 2–10, 2009, doi: 10.1063/1.3176467.
- [44] A. Wolf, P. Pohl, and R. Brendel, “Thermophysical analysis of thin films by lock-in thermography,” *J. Appl. Phys.*, vol. 96, no. 11, pp. 6306–6312, 2004, doi: 10.1063/1.1811390.
- [45] A. Salazar, A. Mendioroz, R. Fuente, and R. Celorrio, “Accurate measurements of the thermal diffusivity of thin filaments by lock-in thermography,” *J. Appl. Phys.*, vol. 107, no. 4, pp. 2–8, 2010, doi: 10.1063/1.3309328.
- [46] F. Cernuschi, A. Russo, L. Lorenzoni, and A. Figari, “In-plane thermal

- diffusivity evaluation by infrared thermography,” *Rev. Sci. Instrum.*, vol. 72, no. 10, pp. 3988–3995, Oct. 2001, doi: 10.1063/1.1400151.
- [47] J. M. Laskar, S. Bagavathiappan, M. Sardar, T. Jayakumar, J. Philip, and B. Raj, “Measurement of thermal diffusivity of solids using infrared thermography,” *Mater. Lett.*, vol. 62, no. 17–18, pp. 2740–2742, Jun. 2008, doi: 10.1016/j.matlet.2008.01.045.
- [48] C. M. Basheer, C. V. Krishnamurthy, and K. Balasubramaniam, “Hot-rod thermography for in-plane thermal diffusivity measurement,” *Meas. J. Int. Meas. Confed.*, vol. 103, pp. 235–240, Jun. 2017, doi: 10.1016/j.measurement.2017.02.022.
- [49] A. ElSheikh, N. Barakat, B. A. Abu-Nabah, and M. O. Hamdan, “Thermal diffusivity estimation in metallic alloys using a one-dimensional flux-based thermography,” *Infrared Phys. Technol.*, vol. 127, no. 1–13, p. 104411, 2022, doi: 10.1016/j.infrared.2022.104411.
- [50] R. M. Lewis, V. Torczon, M. W. Trosset, and C. William, “Direct Search Methods: Then and Now Operated by Universities Space Research Association,” *Science (80-.)*, vol. 124, no. 1–2, pp. 191–207, 2000, [Online]. Available: www.elsevier.nl/locate/cam.
- [51] J. A. Nelder and R. Mead, “A simplex method for function minimization,” *Comput. J.*, vol. 7, no. 4, pp. 308–313, 1965, [Online]. Available: <http://comjnl.oxfordjournals.org/>.
- [52] “Aluminum 2024-T4; 2024-T351,” *MatWeb Material Property Data*. <https://www.matweb.com/search/DataSheet.aspx?MatGUID=67d8cd7c00a04ba29b618484f7ff7524> (accessed Apr. 18, 2022).
- [53] “Specification Sheet: Alloy 304/304L,” *Sandmeyer Steel Company*, 2014. <https://www.sandmeyersteel.com/304L.html#PhysicalProperties> (accessed Jan. 19, 2022).
- [54] R. Usamentiaga, D. F. Garcia, C. Ibarra-Castanedo, and X. Maldague, “Highly accurate geometric calibration for infrared cameras using inexpensive calibration targets,” *Measurement*, vol. 112, no. January, pp. 105–116, 2017, doi: 10.1016/j.measurement.2017.08.027.
- [55] B. Livada and D. Perić, “The influence of the water on scene IR signature,” in

- Target and Background Signatures V*, 2019, vol. 11158, pp. 129–138, doi: 10.1117/12.2532552.
- [56] R. N. Handcock *et al.*, “Thermal infrared remote sensing of water temperature in riverine landscapes,” in *Fluvial Remote Sensing for Science and Management*, P. E. Carbonneau and H. Piégay, Eds. John Wiley & Sons, Ltd, 2012, pp. 85–113.
- [57] H.-Y. Chen and C. Chen, “Determining the emissivity and temperature of building materials by infrared thermometer,” *Constr. Build. Mater.*, vol. 126, no. 2016, pp. 130–137, 2016, doi: 10.1016/j.conbuildmat.2016.09.027.
- [58] E. Lisiecka, “Reduction of the impact of emissivity on high temperature measurements in non-contact thermometric devices,” *Opt. Appl.*, vol. 47, no. 3, pp. 373–381, 2017, doi: 10.5277/oa170304.
- [59] A. Fryskowska-Skibniewska, P. Delis, M. Kedzierski, and D. Matusiak, “The conception of test fields for fast geometric calibration of the FLIR VUE PRO thermal camera for low-cost UAV applications,” *Sensors*, vol. 22, no. 7, p. 2468, 2022, doi: 10.3390/s22072468.
- [60] American Society for Testing and Materials, *ASTM E1933 -14 (2018), Standard practice for measuring and compensating for emissivity using infrared imaging radiometers*. West Conshohocken, Pensilvania, USA: ASTM, 2018.
- [61] Teledyne FLIR, “Use Low-Cost Materials to Increase Target Emissivity,” 2015. <https://www.flir.com/discover/rd-science/use-low-cost-materials-to-increase-target-emissivity/> (accessed Sep. 20, 2022).
- [62] W. Jin, C. Liu, and J. Xiu, “Infrared nonuniformity correction and radiometric calibration technology using U-shaped blackbody,” in *Proceedings of SPIE - International Symposium on Photoelectronic Detection and Imaging 2011: Advances in Imaging Detectors and Applications*, Feb. 2011, vol. 8194, pp. 273–278, doi: 10.1117/12.900122.
- [63] Y. Tendero, S. Landeau, and J. Gilles, “Non-uniformity Correction of Infrared Images by Midway Equalization,” *Image Process. Line*, vol. 2, pp. 134–146, Jul. 2012, doi: 10.5201/ipol.2012.glm-t-mire.
- [64] Z. Zhang, “A flexible new technique for camera calibration,” *IEEE Trans. Pattern Anal. Mach. Intell.*, vol. 22, no. 11, pp. 1330–1334, 2000, doi:

10.1109/34.888718.

- [65] B. A. Abu-Nabah, A. O. ElSoussi, and A. E. R. K. Al Alami, "Simple laser vision sensor calibration for surface profiling applications," *Opt. Lasers Eng.*, vol. 84, pp. 51–61, 2016, doi: 10.1016/j.optlaseng.2016.03.024.
- [66] B. A. Abu-Nabah, A. O. ElSoussi, and A. E. R. K. Al Alami, "Virtual laser vision sensor environment assessment for surface profiling applications," *Measurement*, vol. 113, no. January 2018, pp. 148–160, 2018, doi: 10.1016/j.measurement.2017.08.052.

Vita

Ahmed Elsheikh was born and raised in Jeddah, Kingdom of Saudi Arabia (KSA). He received his primary and secondary education in KSA and was always been interested in the Aerospace field. He joined the Bachelor of Science in Mechanical Engineering at the American University of Sharjah (AUS) in 2016 from which he graduated with a minor in Aerospace Engineering and cum laude honors. During his senior bachelor's study, his teammates and him won the best mechanical senior design project among 10 other projects and co-authored a published journal article. In August 2020, Mr. Ahmed Elsheikh was offered a fully funded scholarship to act as a Graduate Research Assistant (GRA) for the Mechanical Engineering Department while pursuing his Master's degree towards specialization in thermal characterization of Aerospace grade metallic alloys using infrared thermography inspection. His research interests are directed towards nondestructive testing and evaluation, infrared thermography inspection, heat transfer/radiation and geometric thermal camera calibration.